Nano-Structures & Nano-Objects 37 (2024) 101089

Contents lists available at ScienceDirect

Nano-Structures & Nano-Objects

journal homepage: www.elsevier.com/locate/nanoso

Magnetic collective state formation upon tuning the interparticle interactions in ensembles of ultrafine ferrihydrite nanoparticles

Dmitry A. Balaev [a], Aleksandr A. Krasikov [a], Yuriy V. Knyazev [a,*], Roman N. Yaroslavtsev [a,b], Dmitry A. Velikanov [a], Yuriy L. Mikhlin [c], Mikhail N. Volochaev [a], Oleg A. Bayukov [a], Valentina P. Ladygina [b], Sergei V. Stolyar [a,b], Rauf S. Iskhakov [a]

[a] Kirensky Institute of Physics, Federal Research Center KSC SB RAS, Krasnoyarsk 660036, Russia
[b] Federal Research Center KSC SB RAS, Krasnoyarsk 660036, Russia
[c] Institute of Chemistry and Chemical Technology, Federal Research Center KSC SB RAS, Krasnoyarsk 660036, Russia

ARTICLE INFO

Keywords:
Nanoparticle coating
Superspin-glass state
Superparamagnetic blocking
Surface spin subsystem

ABSTRACT

The results of a study of the dynamic (alternating current magnetic susceptibility) and static magnetic properties, as well as ^{57}Fe Mössbauer spectrometry and ferromagnetic resonance of two-line ferrihydrite nanoparticle systems with varying intensities of magnetic interparticle interactions are reported. The strength of the magnetic interparticle interactions has been tuned by coating (with various degrees of coating) the ferrihydrite particles (2–4 nm in size and an average size ~2.7 nm) of the initial synthetic sample by arabinogalactan. Also, a biogenic ferrihydrite sample (an average particle size of 2-nm) with a natural organic coating was studied and it has the weakest magnetic interparticle interactions among of all the samples. Relaxation times of the particle's magnetic moment were determined by the data of static and dynamic magnetic susceptibilities and from analysis of ^{57}Fe Mössbauer spectrometry. Based on the temperature dependences of the relaxation times, it has been concluded that the predominantly collective processes of freezing of the particle magnetic moments occur under the action of the magnetic interparticle interactions. It is shown that an important role in these processes is played by a magnetic subsystem of the surface spins of the particles. The effect of the interplay between the surface spin and magnetic moment subsystems on the static magnetic properties (low-temperature magnetic hysteresis loops) and the parameters of the microwave absorption line under the magnetic resonance conditions is discussed.

1. Introduction

The range of applications for magnetic nanoparticles is being continuously expanded, both in technical and biomedical areas. Along with the evolving ideas about their use in biomedicine and microelectronics [1], magnetic nanoparticles have recently been found promising for ecology as sorbents of heavy elements [2] and for magnetic field-enhanced catalysis [3]. To use nanoparticles in these fields, a fundamental knowledge of their behavior under specific environmental conditions is needed, which requires a comprehensive study of magnetic nanoparticle systems. Here, of great importance are both the search for new synthesis techniques and materials exhibiting magnetic properties at the nanoscale and the targeted magnetic characterization of newly synthesized materials. Due to surface and size effects, nanoparticles acquire new properties which differ from those of their bulk analogs and to properly exploit these effects, various nanoparticle systems should be thoroughly investigated.

At the same time, a real material containing nanoparticles is already an ensembly of particles and its characteristics are determined not only by the individual properties of particles, but also by the properties of the entire ensemble. This manifests itself, first of all, in the impact of the magnetic interparticle interactions (MIPIs), especially in composites highly filled with nanoparticles [4]. Obviously, the MIPIs can become apparent when the interparticle distances are such that the MIPI energy is comparable to the energy of the magnetic anisotropy of an individual particle. The MIPIs can manifest themselves in the response to both an ac magnetic field and a field that changes with a large gradient; if particles are dispersed in a liquid, they will stick together after switching on an external magnetic field. In biomedical applications, e.g., magnetic hyperthermia, the MIPIs drastically affect the value of the heating effect

* Corresponding author.
E-mail address: yuk@iph.krasn.ru (Y.V. Knyazev).

https://doi.org/10.1016/j.nanoso.2023.101089
Received 18 September 2023; Received in revised form 4 December 2023; Accepted 27 December 2023
Available online 5 January 2024

[5]. This MIPI problem has been solved for many years [6–9] and is still urgent when characterizing new magnetic nanomaterials [10–28].

Depending on the distances between particles and features of their crystallochemical properties, the MIPIs can have different origins: magnetic dipole—dipole interactions or direct and indirect exchange of spins of surface atoms of neighboring particles. A reasonable way to purposefully tune the MIPI intensity is the spatial separation of particles. When it is done, a synthesized material is either a composite with particles evenly distributed in a non-magnetic medium or a powder (including that dissolved in a liquid) with particles uniformly coated with a layer of a non-magnetic material.

Using this approach, a system of ferrihydrite nanoparticles with the nominal chemical formula $Fe_2O_3 \times nH_2O$ coated with natural polysaccharide arabinogalactan to different degrees was obtained. Iron oxyhydroxide only exists at the nanoscale. The magnetic moments of the iron atoms in ferrihydrite are ordered antiferromagnetically [29], which causes a weak magnetic response. Meanwhile, due to defects on the surface and in the bulk of the particles, ferrihydrite exhibits the above-mentioned new nanoscale property: an uncompensated magnetic moment [30,31]. Therefore, the magnetic moments of ultrafine (several nanometers) particles attain hundreds of Bohr magnetons and ferrihydrite can be considered to be a magnetically active nanomaterial [32–35]. According to the data on several investigated ferrihydrite powder systems [36–42], the MIPIs affect noticeably their magnetic properties. In [40] the possibility of obtaining synthetic ferrihydrite nanoparticles with an organic (arabinogalactan) coating was demonstrated. In [41] the dynamic magnetic properties (ac magnetic susceptibility) of ferrihydrite systems were investigated. In the cited works, two nanoparticle systems were studied: the initial chemical ferrihydrite with strong MIPIs and chemical ferrihydrite with the MIPIs significantly weakened by coating of the nanoparticles. This study explores a series of samples with different degrees of coating of the initial ferrihydrite with arabinogalactan and, hence, different MIPI effects, and a biogenic ferrihydrite sample with a natural organic coating formed during the vital activity of microorganisms. The central objective of this study was to trace the change in the static and dynamic magnetic properties and the magnetic resonance properties (ferromagnetic resonance and ^{57}Fe Mössbauer spectrometry) of a series of powder systems and to establish the role of the MIPIs in the formation of these properties.

2. Experimental

2.1. Sample preparation

Samples of ferrihydrite nanoparticles with different degrees of coating with arabinogalactan (AG) were obtained by hydrolysis of iron (III) nitrate with dosed addition of AG at one of the stages, which was described in detail in [40,42]. A series of the samples included initial ferrihydrite without AG (sample FH-0) and three samples with different AG contents: FH-1, FH-2 and FH-3. In the synthesis, the individual nanoparticles in both the initial and AG-coated samples were assumed to have a ferrihydrite "core" of the same size. This assumption was supported by electron microscopy, magnetic measurement and Fe^{57} Mössbauer spectrometry data from [38–40,43].

Biogenic ferrihydrite was obtained by cultivating the *Klebsiella oxytoca* bacteria and separating ferrihydrite nanoparticles from the products of their vital activity; the technique used was described in detail in [43,44]. According to the previous results, ferrihydrite nanoparticles with an average size of 2.0 nm have a natural organic coating. This sample is hereinafter referred to as FH-bio. All the samples selected for the investigations (both synthetic ferrihydrite with AG and biogenic ferrihydrite) were powder systems.

2.2. Experimental techniques

The transmission electron microscopy (TEM) investigations were carried out on a Hitachi HT7700 transmission electron microscope at an accelerating voltage of 100 kV. According to the results of the microstructural characterization (see Supplementary materials), the average particle size of the ferrihydrite particles (without taking into account the organic shell) is 2.7 nm for samples FH-0, FH-1, FH-2 and FH-3 and 2.0 nm for sample FH-bio. Selective area electron diffraction (SAED) patterns contain two diffuse rings, which point out that these samples belong to the so-called two-line ferrihydrite.

Mössbauer spectra were obtained on an MS-1104Em spectrometer (Research Institute of Physics, Southern Federal University, Russia) in the transmission geometry with a Co^{57}(Rh) radioactive source, for the temperature range of 4–300 K using a CFSG-311-MESS cryostat, with the sample in the exchange gas based on a closed-cycle Gifford—McMahon cryocooler (Cryotrade Engineering). The modulating signal of motion of the radioactive source was specified by a triangular pulse. The sample, with a relative thickness of 5 mg/cm^2, was placed in 10 μm thick aluminum foil and the obtained pellet was pressed and mounted on a low-temperature insert of the cryostat under continuous evacuation. The spectra were processed in the original software by changing the entire set of hyperfine parameters, using the least squares method in the linear approximation.

The temperature dependences of the ac magnetic susceptibility were measured on a Quantum Design Physical Property Measurement System (PPMS-9) at frequencies of 10, 100, 1000 and 10000 Hz with an ac field amplitude of 2 Oe. The measurements of the temperature dependences of magnetization M in weak dc fields (2, 10, 20 and 50 Oe) were performed on a SQUID magnetometer [45]. The $M(T)$ dependences in stronger fields (0.1–50 kOe) and $M(H)$ hysteresis loops were measured at $T = 4.2$ K on a vibrating sample magnetometer [46]. The $M(T)$ dependences were obtained in the zero-field cooling (ZFC) and field cooling (FC) modes at temperatures obviously higher than the temperature of the irreversible behavior of the magnetization in the specified field. During the magnetic measurements, the investigated powder was fixed in paraffin in a measuring capsule. The magnetization data are presented in emu units reduced to the powder weight.

X-band ferromagnetic resonance (FMR) spectra were recorded on a Bruker ELEXSYS 560 spectrometer at a microwave radiation frequency of ~9.4 GHz in the temperature range of 100–300 K. In these measurements, the powder samples were fixed in epoxy resin.

3. Dynamic properties

3.1. Temperature dependences of the ac susceptibility and low–field magnetization

Fig. 1a shows FC and ZFC temperature dependences of the magnetization M obtained in a probe field of $H = 2$ Oe and temperature dependences of the real part of the ac magnetic susceptibility χ' (the ac field amplitude is 2 Oe) for all the investigated samples. The $\chi'(T)$ dependences contain a peak which shifts to the high-temperature region with the increasing ac field frequency. The dc magnetization maximum under the ZFC conditions corresponds to a lower temperature than the susceptibility peak at a frequency of $f = 10$ Hz. The discrepancy between the ZFC and FC $M(T)$ dependences (i.e., the influence of thermomagnetic prehistory) is observed starting with a temperature somewhat higher than the temperature of the $M(T)_{ZFC}$ maximum.

Due to the uncompensated magnetic moment of the ferrihydrite nanoparticles (see Introduction), the described behavior of the $\chi'(T)$ and $M(T)$ dependences is a typical manifestation of the processes of superparamagnetic unblocking of the particle magnetic moments that occur with the increasing temperature. These processes can be described by the classical N é el—Brown equation at time τ of the particle magnetic moment reversal:

$$\tau = \tau_0 \cdot \exp(K_{eff} \cdot V/kT) \cdot \quad (1)$$

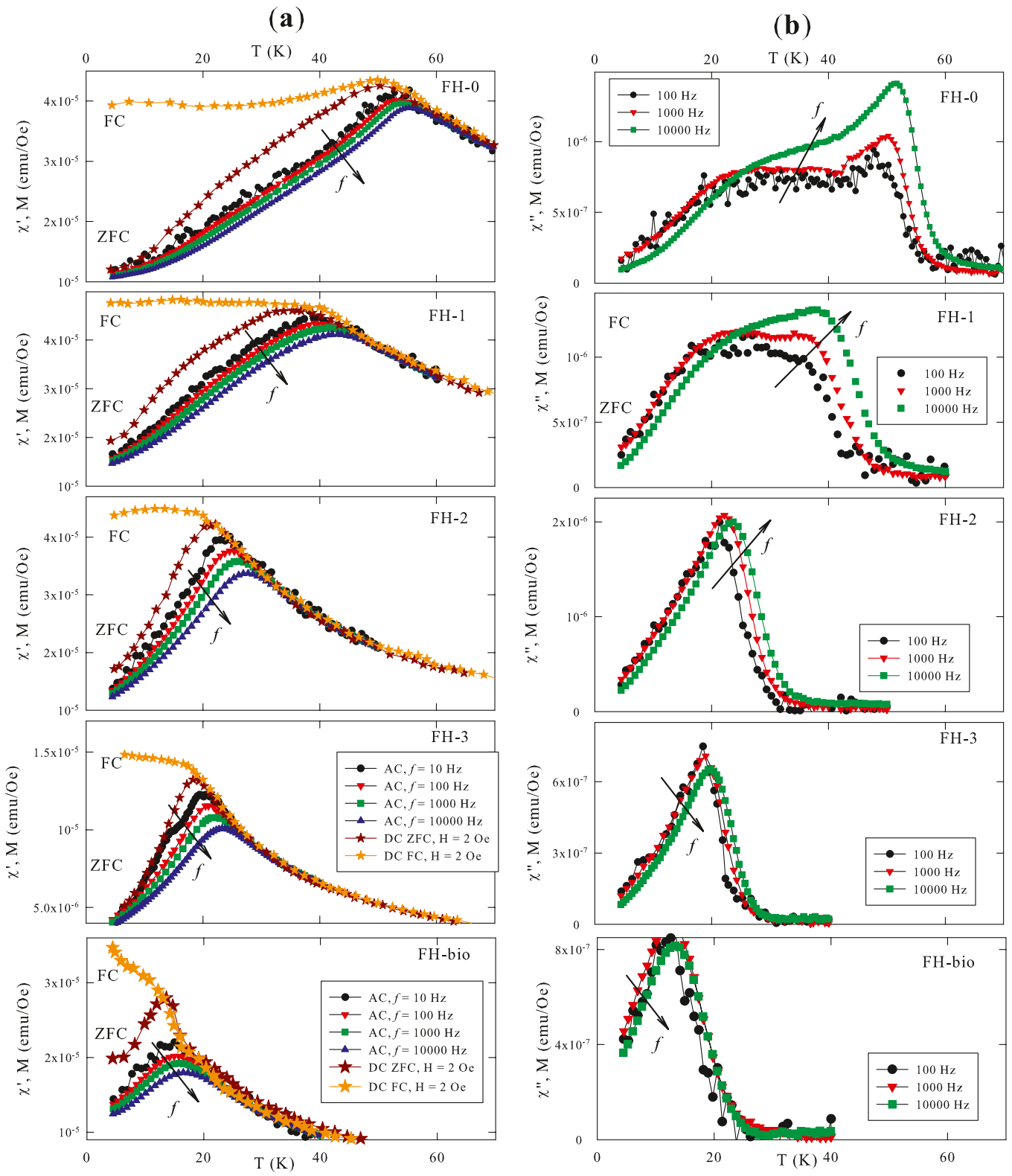

Fig. 1. Temperature dependences of (a) the real part of ac magnetic susceptibility χ' and dc magnetization M under the ZFC and FC (in a field $H = 2$ Oe) conditions (on the left) and (b) imaginary part of ac magnetic susceptibility χ'' (on the right) at frequencies of 10, 100, 1000 and 10000 Hz for the samples under study. The sample weights in the ac and dc measurements were the same. The legend in the bottom figure on the left (a) corresponds to all the data.

Here, τ_0 is the particle magnetic moment relaxation time (usually 10^{-9}–10^{-13} s [31]), K is the magnetic anisotropy constant, V is the particle volume and k is the Boltzmann constant. It follows from Eq. (1) that the superparamagnetic (SPM) blocking temperature is:

$$T_B = K \cdot V / \ln(\tau_m/\tau_0) \cdot k \cdot \quad (2)$$

Formula (2) implies that, at temperature T_B, the characteristic time τ_m of the experimental procedure coincides with τ ($\tau = \tau_m$). In the

magnetic measurements, the τ_m value is determined by the ac field frequency $\tau_m = 1/(2\pi \cdot f)$ and, for static magnetometry, amounts to 10–100 s [31]. The T_B value can approximately be determined as the maximum temperature in the $\chi'(T)$ or $M(T)_{ZFC}$ dependence. In Fig. 1a, one can see a qualitative agreement with the prediction of Eq. (2): with decreasing τ_m, the temperature of the transition to the SPM state increases. Note that in the temperature region starting slightly above the $\chi'(T)$ maximum temperature at the maximum frequency, the $\chi'(T)$ dependences for all the frequencies and the $M(T)$ dependence coincide, which is a sign of the SPM state.

The data presented in Fig. 1a reveal a trend that can be clearly seen when comparing the positions of the $\chi'(T)$ and $M(T)_{ZFC}$ maxima (hereinafter, T_{max}) for different samples: the temperature T_{max} decreases in the series FH-0, FH-1, FH-2, FH-3 and FH-bio. Taking into account the identical size and properties of the particles (see Section 3), this behavior contradicts the prediction of Eq. (2) and is obviously related to the effect of the MIPIs. An increase in the temperature T_{max} and, in fact, in the temperature of the transition to the SPM state are a sign of the impact of the MIPIs in a system of magnetic nanoparticles, as observed by many authors [11,13,15,16,21,23,27]. One can state a monotonic decrease in the temperature T_{max} with the growing amount of added AG, which speaks about an effective decrease in the MIPI influence after coating of the ferrihydrite particles. Interestingly, the data on the sample FH-bio, in which the organic coating was formed during the synthesis, also fall within the scope of the MIPI influence. This sample exhibits the lowest T_{max} values among all the samples, although the difference between the T_{max} values for FH-bio and FH-3 may be caused by the somewhat smaller particle size in the sample FH-bio (see Supplementary materials), according to Eq. (2), in which $T_B \sim V$.

There is another MIPI-related feature in the temperature behavior of the magnetization under the FC conditions. The $M(T)_{FC}$ dependences for samples FH-bio and FH-3 are the functions increasing over the entire temperature range, including the region below T_{max}. Such a shape can be considered classical for non-interacting or weakly interacting particles. With a decrease in the added AG amount (or an increase in the MIPI intensity), the $M(T)_{FC}$ dependences either weakly depend on temperature or decrease with it. The described reshaping of the $M(T)_{FC}$ dependence in the series FH-0, FH-1, FH-2, FH-3 and FH-bio occurs quite monotonically, which also confirms a consistent decrease in the degree of the MIPIs in these samples.

Fig. 1b presents the temperature dependences of the imaginary part of the ac magnetic susceptibility χ''. Let us consider their fairly obvious features. The $\chi''(T)$ maxima shift towards higher temperatures with increasing frequency, while the temperatures of the $\chi''(T)$ maximum are somewhat lower than the T_{max} values in the $\chi'(T)$ dependences measured at the same temperature. For samples FH-0, FH-1, FH-2, FH-3 and FH-bio, the $\chi''(T)$ peaks shift to the low-temperature region monotonically, as the $\chi'(T)$ data present in Fig. 1a. However, there are qualitative differences in the $\chi''(T)$ behavior for the samples, with different degrees of the MIPI effect.

The first thing that catches one's eye is a characteristic $\chi''(T)$ plateau observed for sample FH-0 below the $\chi''(T)$ maximum temperature (Fig. 1b, on the top). This plateau-like shape also appears for sample FH-1. For the other samples, such a plateau is not visualized. In [41], this χ''(T) behavior was modelled for samples FH-0 and FH-3 using a well-known approach [15,16]. It was assumed that the imaginary part of the ac magnetic susceptibility characterizes dissipation in two subsystems: the subsystem of particle magnetic moments (the uncompensated magnetic moments of antiferromagnetically ordered ferrihydrite particles) and the subsystem of surface spins. The peak at high temperatures corresponded to the first subsystem and the plateau (named a shoulder in [47]) was compared with the processes occurring in the surface spin subsystem. The anisotropy energy distribution functions for these subsystems served as fitting parameters. For sample FH-3, in which the MIPI effect is insignificant, the experimental data obtained at different frequencies were described at the same parameters of the anisotropy energy distribution functions of both systems (for a successful fit, it was necessary to take into account the contributions of both subsystems; the contribution of the surface was insignificant). At the same time, when describing the $\chi''(T)$ dependences for the sample FH-0 at different frequencies, it was necessary to change the width of the distribution function of the second subsystem, corresponding to the surface spins. In other words, in the sample in which neighboring particles contact directly, the surface spin subsystem becomes, to a certain extent, common to many particles.

There is another feature [48] that should be noted in the $\chi''(T)$ evolution with a decrease in the MIPI influence. The maximum χ'' value (at the temperature of the distinct $\chi''(T)$ peak) increases with frequency (Fig. 1b). For samples FH-3 and FH-bio, in which the MIPI effect is weak, the maximum χ'' value tends to decrease with the increasing frequency. The described change in the behavior of the χ'' peak amplitude is consistent with the data reported in [48,49].

3.2. Evolution of the Mössbauer spectra

Fig. 3 shows the Mössbauer spectra of the investigated ferrihydrite samples recorded in the temperature range of 4–300 K. At room temperature (Fig. 2a), the spectra of all the samples are paramagnetic doublets consisting of three components, found previously when studying ferrihydrite nanoparticles [50,51]. Since, according to the available neutron diffraction data, the ferrihydrite magnetic ordering temperature is ~350 K [29], the quadrupole form of the spectrum is indicative of the SPM state of the nanoparticles (this was also confirmed by our magnetization measurements). The partial doublets correspond to three non-equivalent positions of iron, with different degrees of local distortions, which are determined in ^{57}Fe Mössbauer spectrometry by the quadrupole splitting (see Table S1). The isomeric shifts of the iron positions point out the trivalent high-spin state of the iron cations. The ratio between the relative areas of these doublets in the spectrum is close to 3:2:1 for all the samples. This means that, in terms of local distortions of the crystal field and the distribution of the iron cations, the nanoparticle coating does not lead to any significant changes in the ferrihydrite structure. At the lowest temperature, 4.2 K (Fig. 2c), the spectra are fully resolved, which indicates blocking of the nanoparticle magnetic moments. The Mössbauer parameters of the spectra are similar and imply the similarity of the magnetic states of the nanoparticles in all the samples. Here, it should be noted that the intensities of spectral line pairs 1–6, 2–5 and 3–4 (the sextet lines are numbered from left to right) for sample FH-bio differ strongly from the characteristic of the powder sample (3:2:1, respectively). This is caused by broadening of the outer lines due to the hyperfine magnetic field distribution [52].

Despite the similarity of the parameters and shape of the spectra at 300 and 4.2 K, the behavior of the samples at intermediate temperatures is essentially different. It is known well that the magnetic moment of SPM nanoparticles is oriented along a certain direction determined by the crystallographic anisotropy — the possible anisotropy of a particle shape [31]. A decrease in temperature leads to the appearance of an allowed Zeeman sextet. However, the dynamics of this process is strongly different due to the MIPI influence, as can be clearly seen in Fig. 2b for the spectra recorded at 30 K. One can see quite distinctly that, at this temperature, sample FH-0 with uncoated particles has a resolved sextet with somewhat broadened outer lines, which indicates the appearance of a certain cone of the total magnetic moment of a particle. This is caused by the thermal fluctuations reflected in Arrhenius-type Eq. (1). As was shown recently [41,42], the formation of a nanoparticle coating leads to a decrease in the number of interacting nanoparticles (in the cluster volume). This is equivalent to a decrease in the number of interacting single magnetic moments on the surface, which lowers the magnetic moment blocking temperature. As a result, at a fixed temperature (30 K), in the samples with the increasing degree of coating (the weakening MIPI effect), one can observe the monotonic broadening of the outer sextet lines during a gradual transition to the relaxation

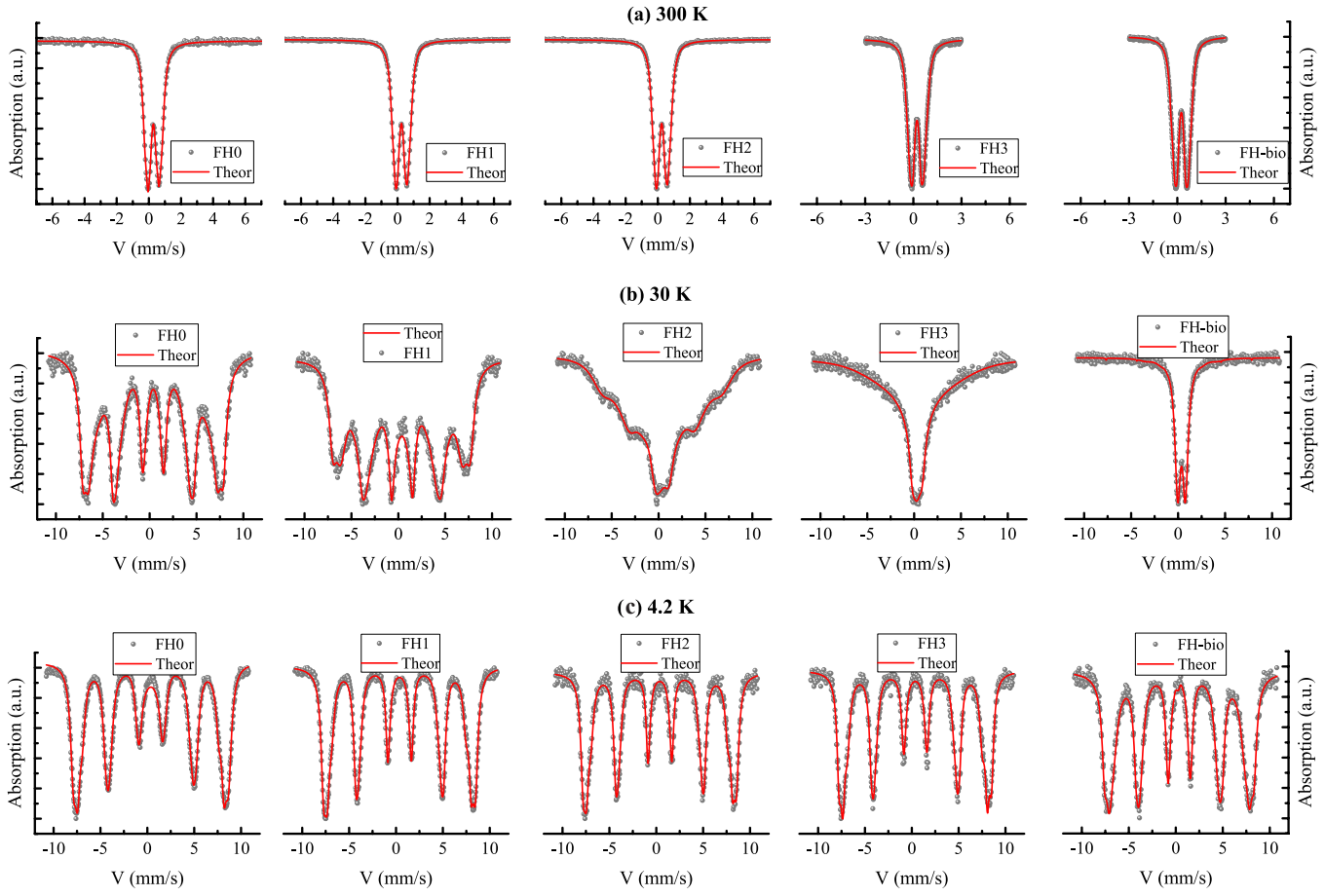

Fig. 2. Mössbauer spectra of the samples at selected temperatures. The experimental spectra are shown by dots; the solid line corresponds to the mathematical processing.

form for sample FH-3 and, further, to the quadrupole doublet shape for sample FH-bio with the highest degree of nanoparticle coating. This allows us to conclude that the MIPIs increase not only the blocking temperature but also the rate of the relaxation process of blocking the nanoparticle magnetic moments.

Let us now turn to the temperature dependences of the average hyperfine magnetic field $<H_{hf}>$, presented in Fig. 3 for all the samples of ferrihydrite nanoparticles with MIPIs of different intensities. One can see a monotonic change in the $<H_{hf}>(T)$ dependence during the formation of a coating on the nanoparticle surface. For samples with the strongest MIPIs (FH-0 and FH-1), the hyperfine magnetic field decreases more slowly than in the samples with a thick particle coating (FH-bio and FH-3). At the same time, in the case of ferrihydrite particles with the natural (FH-bio) and artificial (FH-3) coatings, the hyperfine field behaves similarly. The small discrepancy can be attributed to some fraction of residual interparticle interactions in FH-3. A similar situation is observed for the second pair of samples (FH-0 and FH-1). In order words, the rate of the decrease in $<H_{hf}>$ on iron nuclei changes monotonically upon variation in the MIPI energy. This energy can be estimated using Eq. (3), which takes into account the contribution of energy E_{int} of the interparticle interactions in the linearized temperature dependence of the hyperfine magnetic field [31,53,54]:

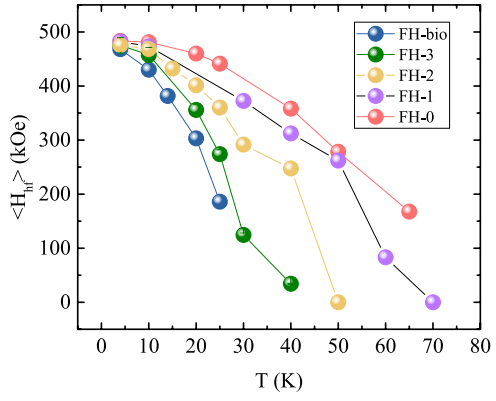

Fig. 3. Temperature dependence of the hyperfine magnetic field for the investigated samples with different degrees of nanoparticle coating. The fitting error is less than the symbol size.

$$\langle H_{hf}\rangle(T) = \langle H_{hf0}\rangle\left(1 - \frac{k_B T}{2KV + E_{\text{int}}}\right) \quad (3)$$

Here, H_{hf} ($T = 4$ K) is the hyperfine magnetic field at the minimum temperature, which, in our experiment, was 4.2 K. Since the particle size in the samples is independent of the degree of coating, it can be assumed that the anisotropy constants K in these nanoparticle ensembles are also similar. Having performed the linearization of the low-temperature portions in Fig. 3, taking into account the angle of inclination, the estimated MIPI energies E_{int} are 157, 98 and 80 k_B for FH-0, FH-1 and FH-2, respectively. It should be noted that, in the samples with the highest degree of natural nanoparticle coating (H-3 and FH-bio), the slope of the $<H_{hf}>(T)$ dependence at $T < T_{\max}$ increases sharply and approaches the limit when the interparticle interactions in the material are completely absent. This case can easily be modelled using Eq. (2) by equating the term E_{int} to zero. Analyzing the residual MIPI energies in samples FH-3 and FH-bio (24 and 7 k_B, respectively), one can assume

that it is extremely difficult to completely get rid of the MIPIs during the formation of an organic coating, and other synthesis methods are needed to eliminate them. At the same time, the preserved interparticle interactions in this case may indicate the retention of some chemical bonds between individual nanoparticles.

The relaxation spectra (see Fig. 2b) can provide information about the relaxation time of the particle magnetic moments [55,56]. Taking into account that the difference between the precession angles in an antiferromagnetic nanoparticle is small, the number of possible precession states is much less than the corresponding number of states of a ferromagnetic nanoparticle [57]. Therefore, the relaxation times of the nanoparticle magnetic moments were determined using the model proposed in [55]. The resulting relaxation times τ, given in Table S1, are used below, in Subsection 3.3.

3.3. Testing of the τ(T) dependences by the Vogel—Fulcher and scaling laws

The temperature T_B is usually considered as the temperature of the transition from the unblocked (SPM) state of the particle magnetic moment at $T > T_B$ to its blocked state at $T < T_B$. The blocking processes in non-interacting particles are described by Eqs. (1) or (2). If particles interact strongly, the transition from the SPM to blocked state can have a collective character; then, the blocked state can be considered as a state of frozen magnetic moments of particles [14,20,25,58]. The individual blocking processes can be distinguished from the collective processes by checking the applicability of Eqs. (1) or (2), or the relationships that take into account the MIPIs to the experimental data.

In our case, the time window for such an analysis at the characteristic particle magnetic moment reversal time τ ($\tau = \tau_m = (2\pi f)^{-1}$, see Subsection 3.1) is ~1.6·(10^{-5}–10^{2}) s, as the unblocking (freezing) temperature, below the maximum temperature T_{max} in the $M(T)_{ZFC}$ and $\chi'(T)$ dependences (Fig.S1) is used. In addition, in Subsection 3.2, using the processing of the relaxation components of the Mössbauer spectra according to the model [55], characteristic times τ at some temperatures were obtained, which can be considered as the times of reversal of the particle magnetic moment. Fig. 4 shows a set of the data obtained for the investigated sample series in the (τ, T) coordinates (the y axis in this figure has a logarithmic scale). One can see a monotonic decrease in the temperature of the transition to the SPM state in the sample series FH-0, FH-1, FH-2, FH-3 and FH-bio for the entire time range used.

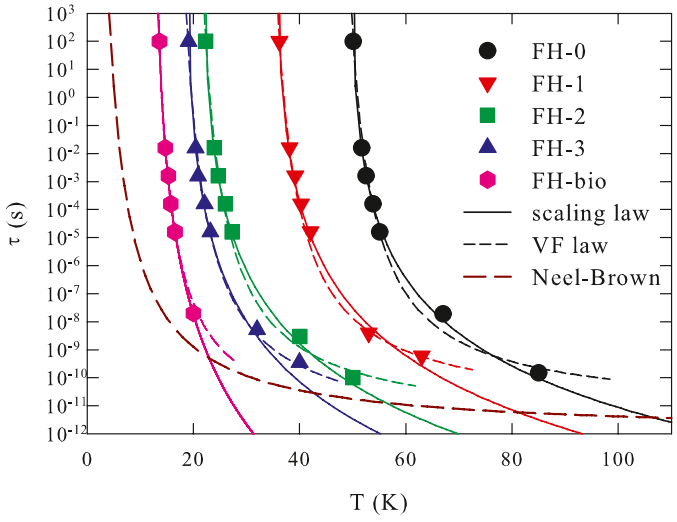

Fig. 4. Temperature dependences of time τ (logarithmic scale) for the investigated samples (symbols). Solid curves show the results of fitting according to the scaling law (6) and short-dashed curves, the results of fitting according to the Vogel—Fulcher law (5). The dependence obtained using Eq. (1) at $K{\cdot}V = 1.44{\cdot}10^{-14}$ erg/cm^3 and $\tau_0 = 10^{-12}$ s is also presented.

Since Eq. (1) can be rewritten in the form.

$$\ln(\tau/\tau_0) = K{\cdot}V/(k{\cdot}T), \quad (4)$$

to check the applicability of Eq. (1), the experimental τ vs T data are plotted in Fig. 5 in the Arrhenius coordinates (the logarithmic scale has been used for τ and the abscissa axis is $1/T$). It can be seen that the experimental data cannot be described by the linear dependence following from (4). This additionally indicates the inapplicability of the approach used for the investigated samples as systems of non-interacting particles.[1]

The simplest way to estimate the energy of the MIPIs is to test the applicability of the phenomenological Vogel—Fulcher law [17]. By analogy with Eq. (4), this law can be written as.

$$\ln(\tau/\tau_0) = K{\cdot}V/(k{\cdot}T - k{\cdot}T_0)\cdot \quad (5)$$

In Eq. (5), the larger the T_0 value, the greater the MIPI contribution. Mathematically, the introduction of T_0 shifts the divergence of Eqs. (1) and (4) from $T = 0$ to T_0. It can be shown that there is certain correspondence between the T_0 value and the MIPI energy if the latter is additive to the magnetic anisotropy energy ($K{\cdot}V$) [39]. There are two criteria for the applicability of Eq. (5) to the experimental results obtained. The first criterion is the straightening of the experimental data in the coordinates $\ln(\tau/\tau_0)$ and $1/(T–T_0)$ at a certain T_0 value; the second criterion is that the τ_0 values fall within a reasonable time range of 10^{-9}–10^{-13} s. Fig. 6 presents an example of the data linearization in the above-mentioned coordinates. The experimental points for each sample fit well to straight lines; therefore, T_0 can be considered to be an independent fitting parameter. The straight lines in Fig. 6 are the results of fitting by Eq. (5) with the already obtained T_0 value. In the fitting procedure, the magnetocrystalline energy $K \bullet V$ was assumed to be the same for samples FH-0, FH-1, FH-2 and FH-3, and can be slightly different for sample FH-bio due to the identity of the properties and particle sizes. The obtained τ_0 values range within 10^{-9}–10^{-13} s (Table 1), which

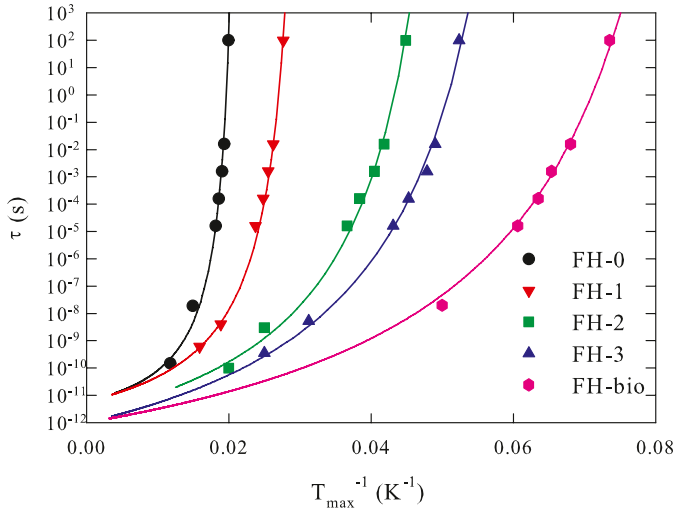

Fig. 5. Dependences of time τ (logarithmic scale) on reciprocal temperature (experimental points T_{max} shown by symbols) for the investigated samples. Solid curves correspond to the fitting according to the Vogel—Fulcher law (5).

[1] If we limit the consideration to the experimental range of times τ corresponding to the measured ac magnetic susceptibility (10^{-2}–10^{-5} s), the linearization of the data from Fig. 4 yields unphysically small τ_0 values in Eq. (4) and the extracted τ_0 values tend to decrease monotonically in the sample series FH-bio, FH-3, FH-2, FH-1 and FH-0. This additionally confirms the enhancement of the MIPI effect in this sample series.

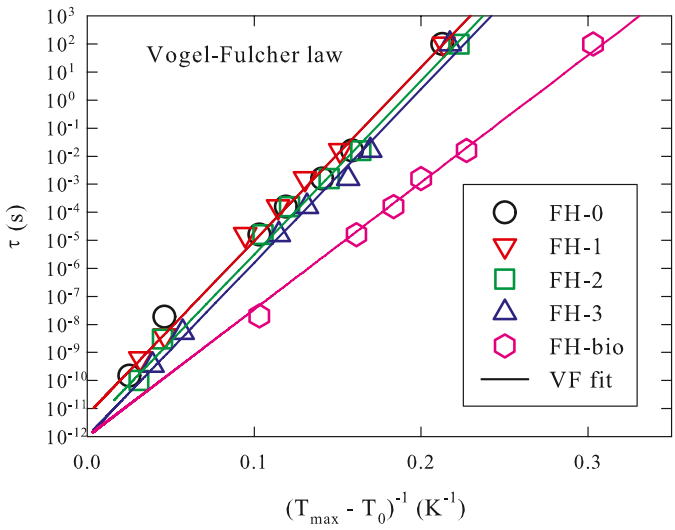

Fig. 6. Linearization of the experimental data (symbols) in the coordinates τ (logarithmic scale) and $1/(T - T_0)$ according to the Vogel—Fulcher law (5). Straight lines correspond to the fitting by Eq. (2) (the R-factor is not less than 0.95). The fitting parameters (including T_0) are given in Table 1.

Table 1
Parameters obtained from the Vogel—Fulcher law (Eq. (5)) and scaling law (Eq. (7)).

	Vogel—Fulcher analysis			Scaling law analysis		
Sample	T_0 (K)	E_A (erg/cm^3)	τ_0 (s)	T_G (K)	$z\nu$	τ_0 (s)
FH-0	45.4	$2{\cdot}10^{-14}$	$6{\cdot}10^{-12}$	49.5	6.75	$1{\cdot}10^{-11}$
FH-1	31.5	$2{\cdot}10^{-14}$	$6{\cdot}10^{-12}$	35.4	7.5	$4{\cdot}10^{-11}$
FH-2	17.8	$2{\cdot}10^{-14}$	$2{\cdot}10^{-12}$	21.5	7.7	$5{\cdot}10^{-10}$
FH-3	14.5	$2{\cdot}10^{-14}$	$1{\cdot}10^{-12}$	18.5	8.0	$2.5{\cdot}10^{-10}$
FH-bio	10.3	$1.45{\cdot}10^{-14}$	$1{\cdot}10^{-12}$	12.75	10.4	$5{\cdot}10^{-11}$

indicates the fulfillment of the second criterion for the applicability of Eq. (5) to the data obtained. Note that the energy values $K\,V$ are typical of ferrihydrite nanoparticles [38–40]. A monotonic decrease in T_0 in the sample series FH-0, FH-1, FH-2, FH-3 and FH-bio (Table 1) indirectly evidences for a monotonic decrease in the MIPI effect in this series. The obtained fitting dependences are also presented in Fig. 6.

If the Vogel—Fulcher law is phenomenological and following the experimental data of dependence (5) is a statement of the existence of MIPIs, then the possible collective nature of the blocking or freezing of the particle magnetic moments can be established from the applicability of the scaling law to spin glasses. As applied to the nanoparticle magnetic moments (in our case, to the uncompensated magnetic moments of ferrihydrite particles), the term superspin glass or superspin glass state (SSG) is used. This scaling law can be written in the form:

$$\tau = \tau_0 \cdot (T/T_{SG} - 1)^{-z\nu}. \quad (6)$$

The functional dependence (6) demonstrates the divergence at the temperature T_{SG}, which, in fact, is the temperature of freezing of the particle magnetic moments or, in other words, the temperature of the transition to the SSG state. In Eq. (6), the value of the combined exponent $z\nu$ [14,20,58] may indicate the implementation of the SSG state. In general, this exponent reflects several important physical parameters: ν is the critical exponent of the correlation length ξ and z is the dynamic index: $\tau \sim \xi^z$ [59]. Thus, the scaling law exponent $z\nu$ can be used to evaluate the effect of interparticle interactions on the rate of relaxation of the nanoparticle magnetic moments during the formation of a spin-glass-like state in the nanoparticle ensemble samples.

The fulfillment of the scaling law (6) by the data obtained is illustrated in Fig. 8, in which the data is plotted in the coordinates τ and $(T/T_{SG} - 1)$ and a double logarithmic scale is used. The straight lines in Fig. 7 show the results of the best fit at the $z\nu$ values indicated in the figure. The τ_0 values are given in Table 1; they are reasonable. The $z\nu$ values (see also Table 1; the $z\nu$ error can be specified as ~0.2) change monotonically as the MIPI strength changes and lie within the limits corresponding to the SSG state[2] [14,20,58,60,61]. The critical indices obtained are similar to those observed earlier for single-crystal samples with the spin-glass behavior [62]. At the same time, the exponent in Eq. (6) for the nanoparticle systems have a fairly wide spread [9,58]. In this regard, it is particularly interesting to establish the origin of this spread. As was shown for a number of core—shell and core—void—shell systems and hollow nanoparticles [58], this exponent increases monotonically and significantly; in addition, the τ_0 parameter decreases by two orders of magnitude [58]. Taking into account that there are no interactions between the nanoparticles, it can be stated that an increase in the $z\nu$ value is directly related to the interactions in a system.

Let us return to the data representation in the direct coordinates τ (logarithmic scale) and T used above in Fig. 4. In addition to the experimental points, in this figure, the Vogel—Fulcher and scaling fits are shown by dashed and solid lines, respectively. In the Vogel—Fulcher law, the τ value approaches the τ_0 value asymptotically. In the scaling law, τ becomes equal to τ_0 at a temperature of about $2T_{SG}$ and then decreases with an increase in T. This limits the time and temperature ranges of applicability of the concept of freezing of the particle magnetic moments (the transition to the SSG state). On the other hand, the $K{\cdot}V$ value obtained above by fitting allows us to model the behavior of the temperature dependence of τ for completely non-interacting particles. Fig. 4 shows such a dependence calculated using the Neel—Brown Eq. (1) at the magnetocrystalline energy value obtained by fitting by the Vogel—Fulcher law ($K \bullet V$ is taken for the sample series FH-0, FH-1, FH-2 and FH-3, see Table 1). It can be concluded from the mutual arrangement of the experimental points and the fitting dependences obtained according to the scaling law and the N é el—Brown equation that, at sufficiently high temperatures, the thermal fluctuations dominate both over the magnetocrystalline anisotropy and the MIPIs. The

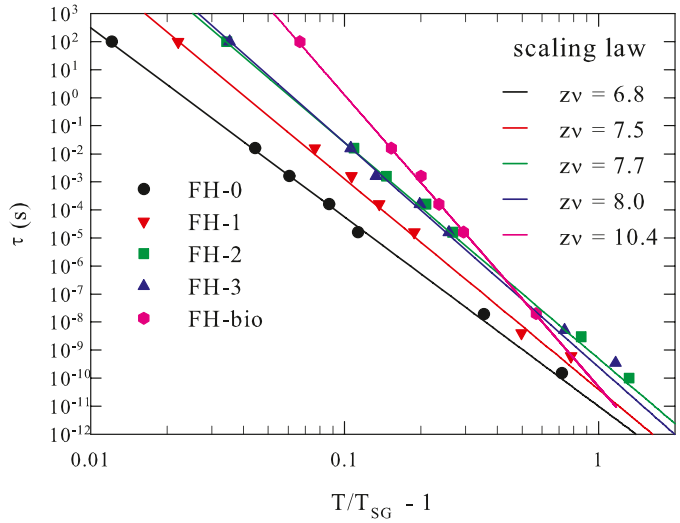

Fig. 7. Dependences of time τ (logarithmic scale) on reduced temperature $T/T_{SG} - 1$ (logarithmic scale) for the investigated samples (symbols). Solid straight lines show the results of fitting according to scaling law (5). The $z\nu$ values used in the fitting are indicated.

[2] Interestingly, weak but retained MIPIs in the sample FH-bio also result in the SSG-like behavior, although, at significantly lower temperatures. The $z\nu$ value is close to the "upper" limit of the range of the SSG state (4–12).

characteristic time of reversal of the particle magnetic moments is $\sim 10^{-12}$ s. As the temperature decreases, the magnetic moments of the particles freeze due to the MIPI contribution, which is well-described within the SSG state. On the other hand, the shape of the temperature dependences of the imaginary magnetic susceptibility of the particles (the presence of a shoulder) reveal an important role of the surface spins in the formation of the SSG state of the particle magnetic moments themselves. In the investigated sample series FH-0, FH-1, FH-2, FH-3 and FH-bio, the effect of the MIPIs and the surface spins weakens monotonically.

Since the organic (artificial) coating reduces the MIPIs, our investigations reliably demonstrate the importance of the surface magnetic moments in the formation of a collective frozen state of magnetic ferrihydrite nanoparticles. This can be considered efficiently as the formation of some granular magnetic material with interacting magnetic grains (nanoparticles). Weakening of the interactions leads to the collapse of the collective state; then, the magnetic behavior of a material is determined directly by the parameters of anisotropy of individual nanoparticles. A similar behavior is observed in bulk spin-glass materials. For example, a neutron scattering study provided direct microscopic evidence for the presence of magnetically correlated spin clusters with an average size of ~2 nm under freezing of the cluster spin glass in the $Ca(Fe_{1/2}Nb_{1/2})O_3$ perovskite [63].

4. Static magnetic properties

4.1. Field dependence of the transition to the unblocked state

A common property of systems of magnetic nanoparticles is a shift of the SPM blocking temperature to the low-temperature region with an increase in the external field. In the previous section, devoted to the description of the dynamic properties of the investigated sample series, the static magnetometry data (ZFC and FC $M(T)$ dependences (Fig. 1a)) in a field of $H = 2$ Oe were also presented. Taking into account the evidence for the SSG state obtained in Subsection 3.3, here, instead of the SPM blocking/unblocking terms, the freezing/thawing of the particle magnetic moments should rather be used. Usually, it is the temperature of the $M(T)_{ZFC}$ maximum that characterizes these processes. The results reported in [42] for samples FH-0, FH-1, FH-2 and FH-3 in fields from 100 to 30 kOe confirmed that the external field affects the shift of the temperature T_{max} somewhat differently at different MIPI contributions. Indeed, in a field of $H = 2$ Oe (Fig. 1a), the difference between the T_{max} values for samples FH-0 and FH-bio is ~46.4 K, while in a field of $H = 5$ kOe, this difference is already 23 K. This is illustrated in Fig. 8.[3] In addition, this figure shows the data obtained for the sample FH-0 at $H = 50$ kOe (inset in Fig. 8a) and for sample FH-bio at $H = 10$ and 30 kOe (inset in Fig. 8c; in fields of up to 4.2 K, the $M(T)_{ZFC}$ maximum for sample FH-bio is already absent).

This study presents the resulting $T_{max}(H)$ dependences obtained in external fields from 2 Oe to 50 kOe for all the samples, including FH-bio. They are shown in Fig. 9 (inset), in which the abscissa axis is logarithmic. It can be seen that, in sufficiently strong fields (5 kOe and more), the difference between the T_{max} values of different samples (in K) becomes somewhat smaller than in a weak field. The main plots in Fig. 9 are the dependences of T_{max} normalized to $T_{max}(H = 2$ Oe) on external field H (logarithmic scale). These data allow us to conclude that, in the case of the strongest MIPIs (sample FH-0), the normalized $T_{max}(H)$ dependence is qualitatively different from similar dependences for the samples with the weak MIPIs. In fields of up to 10^3 Oe, the T_{max} value for sample FH-0 is almost field-independent (even a slight T_{max} growth is observed in fields of hundreds of Oe) and only further, with increasing H, does the T_{max} value drop. For sample FH-1, the T_{max} values in fields of 2 and 20 Oe are approximately the same, while in stronger fields T_{max}

[3] The data presented in Fig. 9 were not reported in [42].

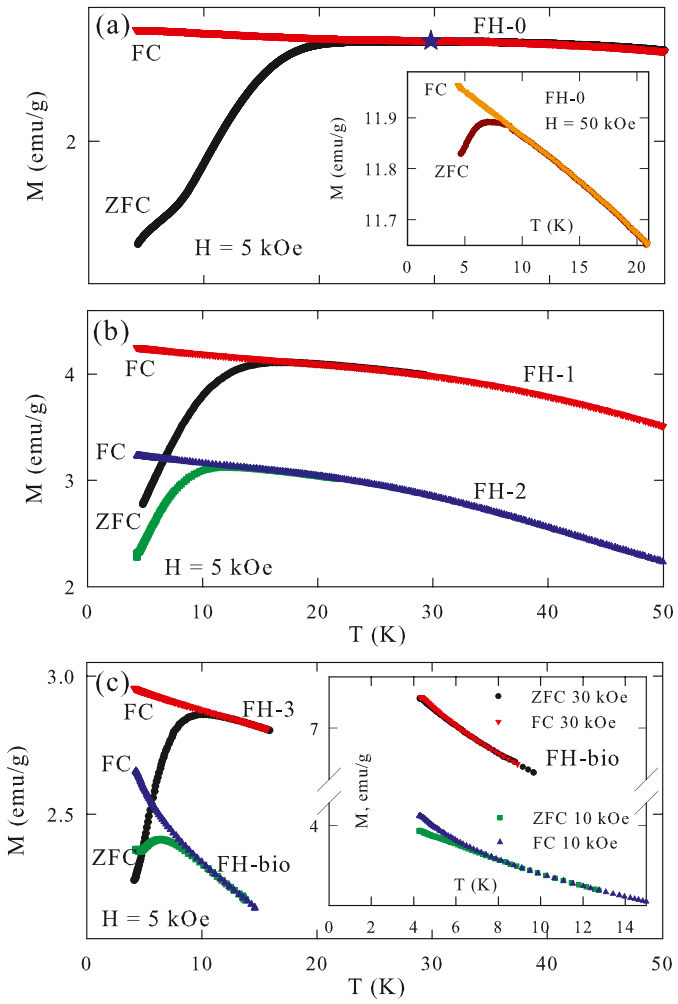

Fig. 8. ZFC and FC temperature dependences of magnetization M in a field of $H = 5$ kOe for samples (a) FH-0, (b) FH-1 and FH-2, and (c) FH-3 and FH-bio. Inset to (a): $M(T)_{ZFC}$ and $M(T)_{FC}$ dependences for sample FH-0 at $H = 50$ kOe. Inset to (b): $M(T)_{ZFC}$ and $M(T)_{FC}$ dependences for sample FH-bio at $H = 10$ and 30 kOe. The asterisk position in (a) corresponds to the temperature T_{max} in the $M(T)_{ZFC}$ dependence.

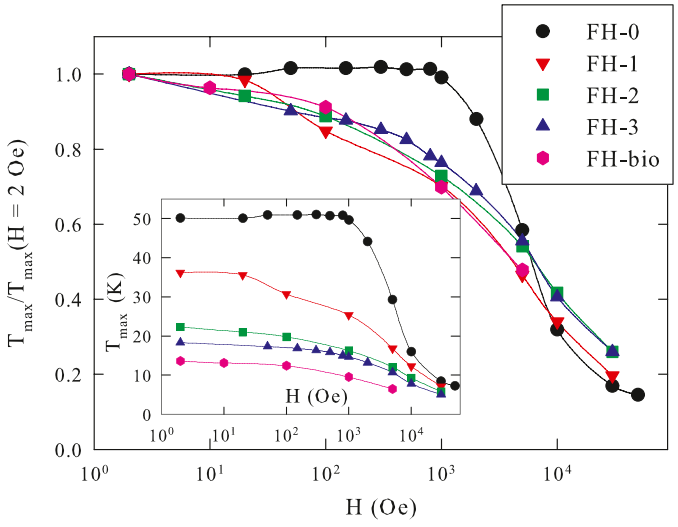

Fig. 9. Field dependences of the $M(T)_{ZFC}$ maximum temperature T_{max} (logarithmic scale) normalized to the T_{max} value at $H = 2$ Oe for the investigated samples. The inset shows the $T_{max}(H)$ dependences (H is the logarithmic scale).

decreases. The normalized $T_{max}(H)$ dependences for samples FH-1, FH-2, FH-3 and FH-bio behave similarly. Therefore, in addition to the effect of the MIPIs on the T_{max} value (see Subsection 3.1), the MIPIs also affect the T_{max} shift toward lower temperatures with the increasing external field, i.e., $T_{max}(H)$ dependence. In sufficiently strong fields (5 kOe and more), T_{max} decreases by approximately the same factor for all the samples.

The magnetic moments of particles in the frozen state are not only affected by the magnetic anisotropy of the individual particles (the energy $K{\cdot}V$), but a non-uniform spatial distribution of the fields of scattering from the magnetic moments of particles is apparently implemented. The magnetic moment per ferrihydrite particle is 150–200 Bohr magnetons [31–33,35,37,39] and the Zeeman energy of such a magnetic moment in a field of ~10^3 Oe is 5–10 K. Possibly, under the ZFC conditions, energy lower than this value is insufficient to destroy the frozen state of the system of the particle magnetic moments at temperatures below T_{max} in a weak field (2 Oe). In Subsection 3.1, it was shown, using the behavior of the imaginary part of the ac susceptibility (Fig. 1b), that the surface spin subsystem dominates in establishing the frozen state. It can be assumed with a high degree of certainty that it is the interaction between the subsystems of the surface spins and magnetic moments of particles that gives rise to the atypical dependence (almost field-independent) of the T_{max} temperature on the external field in the range of up to 10^3 Oe for the sample with the strongest MIPI effect (FH-0).

4.2. Magnetic hysteresis loops

Obviously, a system of magnetic nanoparticles in the blocked state should exhibit magnetic hysteresis. The magnetization hysteresis loops for the investigated samples at $T = 4.2$ K are shown in Fig. 11 (in this figure, the data for samples FH-1, FH-2, FH-3 and FH-bio are shifted along the y axis by –10, –20, – 30 and –40 emu/g, respectively). The shape of the $M(H)$ dependences is typical of systems of antiferromagnetic nanoparticles [35,61–63] and, according to a number of works, can approximately be described by several terms:

$$M(H) = M_{FM}(H) + M_{SS}(H) + M_{AFM}(H)\cdot \quad (8)$$

The first term is the ferromagnetic component, reflecting the behavior of the uncompensated magnetic moments of particles (in the SPM state, $M_{FM}(H)$ is described by the Langevin function). The second term is the magnetic response from the subsystem of surface spins [35,64–66]; at temperatures well above T_{max}, the $M_{SS}(H)$ dependence is described by the Brillouin function. The processing of the $\chi''(T)$ dependences showed that, in addition to the transition of the magnetic moments of particles to the SSG state, the subsystem of surface spins is frozen (see Subsection 3.3). At low temperatures, the magnetic response from this subsystem can be considered to be approximately linear with respect to the field [67], although spin glasses also exhibit magnetization hysteresis [49]. Finally, the third term, $M_{AFM}(H)$, corresponds to the antiferromagnetic susceptibility of the particles themselves (the particle cores) [64–66]. The $M_{AFM}(H)$ dependence, in the first approximation, is linear with respect to field, similar to an antiferromagnet with a random distribution of the crystallographic axes.

The main feature observed in Fig. 10 is a decrease in the coercivity H_C in the sample series FH-0, FH-1, FH-2, FH-3 and FH-bio (the H_C values at $T = 4.2$ K in this sample series are 4.1, 2.6, 1.9, 1.7 and 1.0 kOe). Taking into account the identity of the particle sizes (at least for FH-0, FH-1, FH-2 and FH-3) and the above-established weakening of the MIPI effect (see Subsection 3) in this sample series, it can be concluded that it is the presence of the MIPIs that leads to an increase in the coercivity. To explain such a strong impact of the MIPIs on the H_C value, it is necessary to investigate the possible nature of the MIPIs. The energy of the magnetic dipole—dipole interactions (with an allowance for 10–12 nearest neighboring nanoparticles) in synthetic ferrihydrite

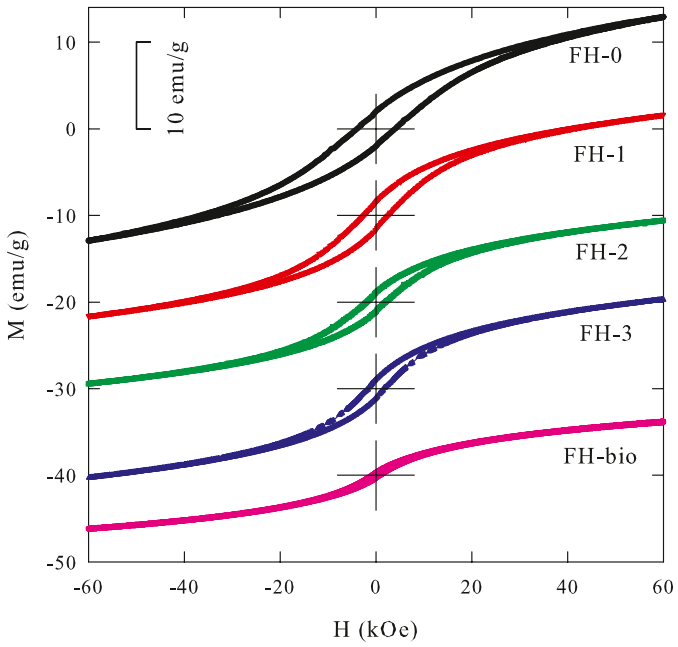

Fig. 10. $M(H)$ hysteresis loops for the investigated samples at $T = 4.2$ K. The data for samples FH-1, FH-2, FH-3 and FH-bio are shifted along the y axis by –10, –20, –30 and –40 emu/g, respectively.

(in fact, in sample FH-0) is no higher than 10 K [41,42]; therefore, here, a direct or indirect exchange (or super-exchange) between atoms of neighboring particles should be considered [31]. This exchange should be implemented precisely through surface atoms, since their bond with the particle core is weakened. In addition, surface atoms are external with respect to the particle; therefore, the shortest chains of exchange couplings are implemented precisely through surface atoms. The role of the spins of surface atoms in the established SSG state was found from the $\chi''(T)$ dependences (see Subsections 3.1 and 3.3, and [41]); the interplay of the subsystems of surface spins and magnetic moments of particles apparently causes the observed coercivity growth in the sample series FH-3, FH-2, FH-1 and FH-0. In other words, the first two terms in Eq. (8) become interrelated at $T < T_{max}$. A similar conclusion was drawn from the pulsed magnetization switching in NiO nanoparticles [69]. Note that, in Fig. 10, in addition to the monotonic change in the H_C value, it can be seen that the field corresponding to the irreversible $M(H)$ behavior also changes. At least for samples FH-bio and FH-3, one can speak about a closed hysteresis loop at a maximum applied field of 60 kOe. However, the hysteresis loops for samples FH-0 and FH-1 are open. The interaction between the particle magnetic moments through the surface spins and the interaction between the subsystems of the particle moments and surface spins can give rise to the irreversible behavior of the magnetization. The apparent drop of the magnetic moment in the sample series FH-0, FH-1, FH-2, FH-3 and FH-bio is most likely due to a smaller amount of ferrihydrite and, consequently, a greater amount of polysaccharide.

5. X-band magnetic resonance

The ferromagnetic resonance (FMR) technique is widely used to characterize and study the magnetic state of magnetic nanoparticle systems [70–93]. However, parameters of observed FMR spectra often cannot be interpreted with confidence. It was demonstrated in the previous sections how the dynamic and static magnetic properties of systems of ferrihydrite nanoparticles change upon variation in the MIPI intensity. Therefore, based on these results, one can compare the parameters of the FMR spectra for the investigated samples and find the variation in these parameters with the change in the MIPI intensity.

Typical FMR spectra are presented in Fig. 11 (at temperatures around (a) 130 and (b) 255 K). The spectra of samples FH-0, FH-1, FH-2 and FH-3 are single Lorentzian lines. The spectra of sample FH-bio can be described by two Lorentzian lines.

Fig. 12 shows temperature dependences of the parameters of the FMR spectra obtained from the processing of the Lorentzian curves: linewidth ΔH (Fig. 11a), resonance field H_R (inset in Fig. 12b) and integral intensity I normalized to the value at $T = 290$ K. The resonance field at 100–300 K ranges only within several tens of Oe and changes slightly from one sample to another. The largest linewidth is observed for the sample FH-0; for the remaining samples (including line 1 for the sample FH-bio), the ΔH values and their temperature dependences are approximately the same. Accordingly, the strong MIPIs lead to a significant broadening of the FMR spectra. In single-domain magnetic nanoparticles, the particle magnetic moments precess under the magnetic resonance conditions; in ferrihydrite, the uncompensated magnetic moments do. Under the resonance conditions, the surface spins coupled weakly to the magnetically ordered particle core also precess. The FMR linewidth is strongly affected by local (scattering) fields induced by the magnetic moments of neighboring particles [80,81]. As the temperature decreases, the role of local fields becomes more significant, which manifests itself in the ΔH growth. Under the MIPI conditions, the developed particle surface should lead to a strong inhomogeneity of local fields and, consequently, to broadening of the resonance absorption line. This can explain the larger linewidth for sample FH-0. The inhomogeneity of local fields apparently manifests itself in the direct contact of particles, which is observed in sample FH-0. When the FMR spectrum is recorded, the interacting particles are affected not only by an external magnetic field, but also by the scattering magnetic fields induced by neighboring nanoparticles. These scattering fields are spatially inhomogeneous and decrease as $1/r^3$ with the increasing distance from the particle center. The effect of these fields manifests itself differently for particles of different sizes. In sufficiently coarse (20–40 nm) particles, only the particle regions that are in direct contact with neighboring particles experience the effect of the scattering fields. In this case, the scattering fields only lead to the appearance of an additional low-intensity absorption line in the FMR spectrum, the resonance field of which is weaker than that of the main line [80,81]. In the case of fine nanoparticles, the entire particle volume is obviously affected by the inhomogeneous scattering field of neighboring particles. In addition, it is important that, with a small spread of particle sizes, close-packed structures can form, so that each particle is affected by inhomogeneous scattering fields of 10–12 neighboring particles. All this causes a strong broadening of the FMR absorption line of fine nanoparticles. According to the experimental data, the ΔH values for the remaining samples with suppressed MIPIs are approximately the same.

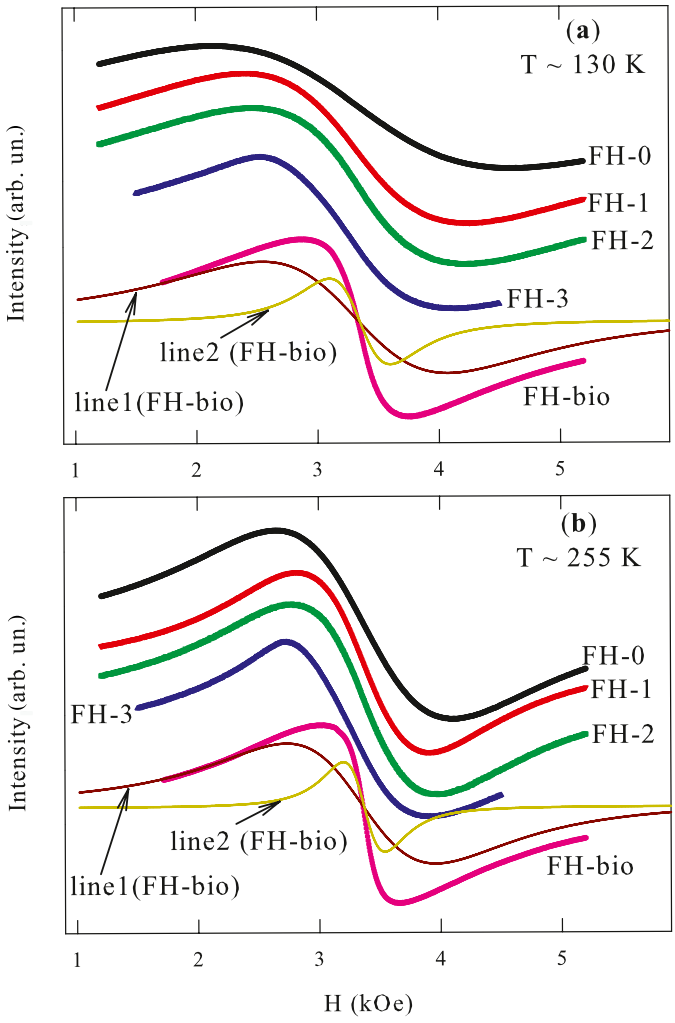

Fig. 11. FMR spectra of the investigated samples at relatively (a) low and (b) high temperatures. The temperatures indicated in (a) and (b) are averaged. The spectra in (a) were obtained at $T = 130$, 129, 126, 139 and 135 K and the spectra in (b), at $T = 251$, 256, 259, 254 and 254 K for samples FH-0, FH-1, FH-2, FH-3 and FH-bio, respectively. Thin lines show the results of processing of the spectra for sample FH-bio by two Lorentzian lines (line 1 and line 2).

The integrated intensity of the absorption lines decreases monotonically with the increasing temperature (Fig. 12b). The non-monotonic behavior of the $I(T)$ dependence was reported in [75,77,78,88–90] and interpreted as a transition to the SPM state, since the integrated intensity is proportional to the magnetization. In the FMR technique, the characteristic measurement time τ_m (in Eqs. (1), (2)) is considered to be inversely proportional to the microwave field frequency [49,68–71]. For the investigated ferrihydrite samples, no pronounced maximum is observed in the $I(T)$ dependence (including line 1 for the sample FH-bio) above 100 K. Possibly, the processes of freezing of the particle magnetic moments, as well as the surface spins, occur at lower temperatures; moreover, under the resonance conditions, the particle magnetic moments are in an external field, which shifts the temperature of the transition to the unblocked state toward lower temperatures. In addition, the $I(T)$ maximum possibly smears due to the distribution over the particle magnetic moments.

Concerning the need for two Lorentzian lines to describe the spectra of the sample FH-bio, the parameters of line 1 are similar to those for the other samples (see Fig. 12). In sample FH-bio, the average particle size is smaller; in such fine ferrihydrite particles, a core—shell structure is pronounced even under the weak MIPIs [43]. Line 2 can be interpreted as a response from the surface spins.

Thus, the main effect of the MIPIs on the shape and parameters of the FMR spectra can be considered to be a significant broadening of the resonance absorption line for sample FH-0, in which particles contact directly. In the case of particles coated with arabinogalactan, the linewidth decreases and remains approximately the same for all the investigated samples.

6. Conclusions

In the investigated series of powder systems of ferrihydrite nanoparticles with different degrees of organic coating, the effect of the MIPIs gradually weakens in the sample series FH-0, FH-1, FH-2, FH-3 and FH-bio. In this series, particles in the samples FH-1, FH-2 and FH-3 were coated with arabinogalactan, while in the biogenic sample FH-bio, the ferrihydrite particles had a natural organic coating formed under the nanoparticle synthesis conditions. A conclusion about a monotonic change in the MIPI intensity was drawn from the comparative analysis of the dynamic and static magnetic properties of the investigated systems, which consist of ferrihydrite nanoparticles with the same size and similar magnetic properties. The temperature of the transition from the

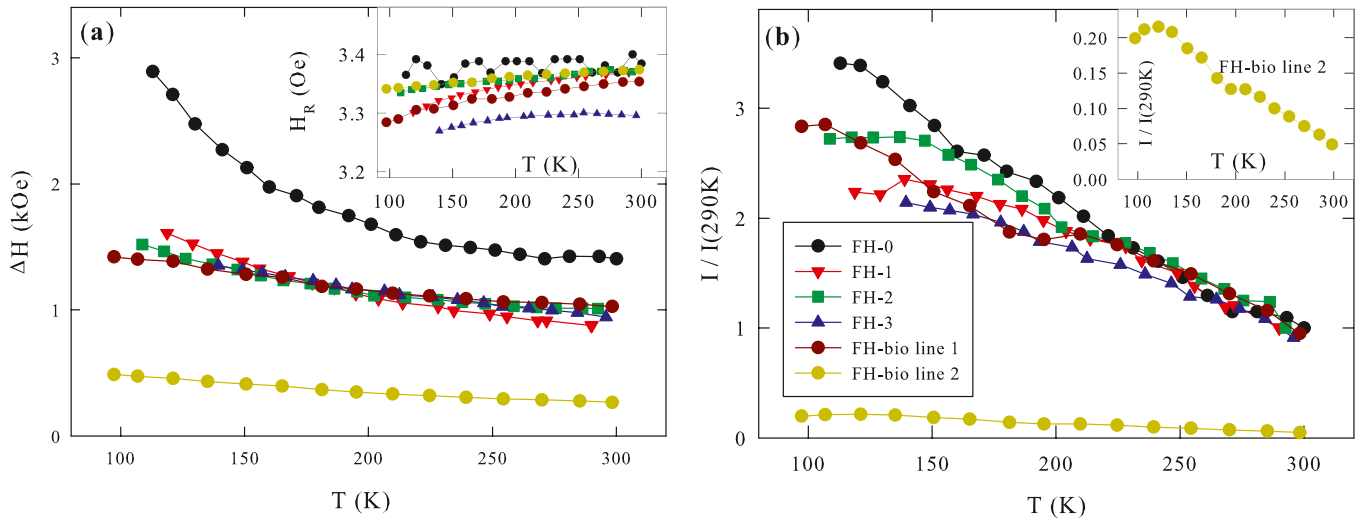

Fig. 12. Temperature evolution of parameters of the FMR spectra: (a) linewidth $\Delta H(T)$ and resonance field $H_R(T)$ (inset in (a)) and (b) relative integrated intensity $I(T)/I(290\ K)$ (insert in (b): $I(T)/I(290\ K)$ for line 2 of the sample FH-bio). The legend in (b) is consistent with the data in (a).

SPM to blocked state shifts by tens of degrees, comparing the behaviors of the extreme samples in the series.

The analysis of the temperature dependences of relaxation times τ (the characteristic time of reversal of the particle magnetic moment ranging from 10^{-10} to 10^{2} s) showed that, as applied to the investigated systems, one can speak mainly about the collective effects of freezing of the particle magnetic moments, i.e., the SSG-type state. Exponents $z\nu$ in the scaling law (6) correspond to spin-glass behavior; it was found that the $z\nu$ value increases smoothly with the decreasing MIPI intensity (Table 1). The observed evolution of the ac susceptibility and hysteresis loops upon variation in the MIPI intensity is indicative of a significant role played by the surface spin subsystem in the collective processes of freezing of the particle magnetic moments. Moreover, the strong MIPI in the initial synthetic ferrihydrite (sample FH-0) leads to a significant increase in the FMR linewidth. These properties can be explained considering the collective effect of surface spins of neighboring particles and, consequently, the effect of local fields on the unblocking and resonance absorption processes.

Funding

This study was carried out within the State Assignment for the Kirensky Institute of Physics of Federal Research Center "Krasnoyarsk Scientific Center", Siberian Branch of the Russian Academy of Sciences and the synthesis of the samples was carried out within the State Assignment for "Krasnoyarsk Scientific Center", Siberian Branch of the Russian Academy of Sciences.

CRediT authorship contribution statement

Mikhlin Yuriy L.: Investigation, Visualization. **Velikanov Dmitry A.:** Investigation, Resources. **Bayukov Oleg A.:** Investigation, Software, Supervision. **Volochaev Mikhail N.:** Investigation, Software, Visualization. **Iskhakov Rauf S.:** Supervision, Validation. **Stolyar Sergei V.:** Investigation, Resources. **Balaev Dmitry A.:** Conceptualization, Formal analysis, Investigation, Resources, Visualization, Writing – original draft, Writing – review & editing, Supervision, Validation. **Ladygina Valentina P.:** Investigation. **Krasikov Aleksandr A.:** Data curation, Investigation, Software. **Yaroslavtsev Roman N.:** Investigation. **Knyazev Yuriy V:** Conceptualization, Data curation, Investigation, Software, Writing – original draft, Writing – review & editing, Formal analysis, Visualization.

Declaration of Competing Interest

The authors declare that they have no known competing financial interests or personal relationships that could have appeared to influence the work reported in this paper.

Data availability

No data was used for the research described in the article.

Acknowledgments

The authors thank M.N. Volochaev for the TEM investigations. The ac magnetic susceptibility measurements and the FMR (Bruker ELEXSYS 560 spectrometer) and TEM studies were carried out on the equipment of the Center for Collective Use, Krasnoyarsk Scientific Center, Siberian Branch of the Russian Academy of Sciences.

Appendix A. Supporting information

Supplementary data associated with this article can be found in the online version at doi:10.1016/j.nanoso.2023.101089.

References

[1] H.A. Khan, M.K. Sakharkar, A. Nayak, U. Kishore, A. Khan, Nanoparticles for biomedical applications: An overview, Nanobiomaterials (2018) 357–384, https://doi.org/10.1016/B978-0-08-100716-7.00014-3.
[2] M. Engel, J.S.L. Pacheco, V. Noël, K. Boye, S. Fendorf, Organic compounds alter the preference and rates of heavy metal adsorption on ferrihydrite, 141485, Sci., Total Environ. 750 (2021), https://doi.org/10.1016/j.scitotenv.2020.141485.
[3] L.M. Martínez-Prieto, J. Marbaix, J.M. Asensio, C. Cerezo-Navarrete, P.-F. Fazzini, K. Soulantica, B. Chaudret, A. Corma, Ultrastable magnetic nanoparticles encapsulated in carbon for magnetically induced catalysis, ACS Appl. Nano Mater. 3 (2020) 7076–7087, https://doi.org/10.1021/acsanm.0c01392.
[4] J. Mohapatra, M. Xing, J.P. Liu, Inductive thermal effect of ferrite magnetic nanoparticles, Materials 12 (2019) 3208, https://doi.org/10.3390/ma12193208.
[5] A. Ali, T. Shah, R. Ullah, P. Zhou, M. Guo, M. Ovais, Z. Tan, Y. Rui, Review on recent progress in magnetic nanoparticles: Synthesis, characterization, and diverse applications, Front. Chem. 9 (2021) 629054.
[6] J.I. Gittleman, B. Abeles, S. Bozowski, Superparamagnetism and relaxation effects in granular Ni-SiO_2 and Ni-Al_2O_3 films, Phys. Rev. B. 9 (1974) 3891, https://doi.org/10.1103/PhysRevB.9.3891.
[7] S. Mørup, M.B. Madsen, J. Franck, J. Villadsen, C.J.W. Koch, A new interpretation of Mössbauer spectra of microcrystalline goethite: "Super-ferromagnetism" or "super-spin-glass" behaviour? J. Magn. Magn. Mater. 40 (1983) 163–174, https://doi.org/10.1016/0304-8853(83)90024-0.
[8] S. Mørup, E. Tronc, Superparamagnetic relaxation of weakly interacting particles, Phys. Rev. Lett. 72 (1994) 3278, https://doi.org/10.1103/PhysRevLett.72.3278.

[9] C. Djurberg, P. Svedlindh, P. Nordblad, M.F. Hansen, F. Bødker, S. Mørup, Dynamics of an interacting particle system: evidence of critical slowing down, Phys. Rev. Lett. 79 (1997) 5154, https://doi.org/10.1103/PhysRevLett.79.5154.

[10] J.M. Vargas, W.C. Nunes, L.M. Socolovsky, M. Knobel, D. Zanchet, Effect of dipolar interaction observed in iron-based nanoparticles, 184428, Phys. Rev. B. 72 (2005), https://doi.org/10.1103/PhysRevB.72.184428.

[11] H. Shim, P. Dutta, M.S. Seehra, J. Bonevich, Size dependence of the blocking temperatures and electron magnetic resonance spectra in NiO nanoparticles, Solid State Commun. 145 (2008) 192–196, https://doi.org/10.1016/j.ssc.2007.10.026.

[12] A.M. Pereira, C. Pereira, A.S. Silva, D.S. Schmool, C. Freire, J.-M. Greneche, J. P. Araujo, Unravelling the effect of interparticle interactions and surface spin canting in γ-Fe_2O_3@SiO_2 superparamagnetic nanoparticles, 114319, J. Appl. Phys. 109 (2011), https://doi.org/10.1063/1.3583652.

[13] D. Caruntu, G. Caruntu, C.J. O'Connor, Magnetic properties of variable-sized Fe_3O_4 nanoparticles synthesized from non-aqueous homogeneous solutions of polyols, J. Phys. D. Appl. Phys. 40 (2007), https://doi.org/10.1088/0022-3727/40/19/001.

[14] M. Suzuki, S.I. Fullem, I.S. Suzuki, L. Wang, C.J. Zhong, Observation of superspin-glass behavior in Fe_3O_4 nanoparticles, Phys. Rev. B Condens. Matter Mater. Phys. 79 (2009), https://doi.org/10.1103/PhysRevB.79.024418.

[15] M. Knobel, W.C. Nunes, H. Winnischofer, T.C.R. Rocha, L.M. Socolovsky, C. L. Mayorga, D. Zanchet, Effects of magnetic interparticle coupling on the blocking temperature of ferromagnetic nanoparticle arrays, J. Non Cryst. Solids 353 (2007) 743–747, https://doi.org/10.1016/j.jnoncrysol.2006.12.037.

[16] W.C. Nunes, L.M. Socolovsky, J.C. Denardin, F. Cebollada, A.L. Brandl, M. Knobel, Role of magnetic interparticle coupling on the field dependence of the superparamagnetic relaxation time, 212413, Phys. Rev. B. 72 (2005), https://doi.org/10.1103/PhysRevB.72.212413.

[17] S. Mørup, M.F. Hansen, C. Frandsen, Magnetic interactions between nanoparticles, Beilstein J. Nanotechnol. 1 (2010) 182–190, https://doi.org/10.3762/bjnano.1.22.

[18] C.A.M. Vieira, R.C. Gomes, F.G. Silva, A.L. Dias, R. Aquino, A.F.C. Campos, J. Depeyrot, Blocking and remanence properties of weakly and highly interactive cobalt ferrite based nanoparticles, J. Phys. Condens. Matter 31 (2019) 175801, https://doi.org/10.1088/1361-648X/ab0353.

[19] F. Fabris, K.-H. Tu, C.A. Ross, W.C. Nunes, Influence of dipolar interactions on the magnetic properties of superparamagnetic particle systems, 173905, J. Appl. Phys. 126 (2019), https://doi.org/10.1063/1.5125595.

[20] K. Nadeem, H. Krenn, T. Traußnig, R. Würschum, D.V. Szabó, I. Letofsky-Papst, Effect of dipolar and exchange interactions on magnetic blocking of maghemite nanoparticles, J. Magn. Magn. Mater. 323 (2011) 1998–2004, https://doi.org/10.1016/j.jmmm.2011.02.041.

[21] M. Tadic, D. Nikolic, M. Panjan, G.R. Blake, Magnetic properties of NiO (nickel oxide) nanoparticles: Blocking temperature and Neel temperature, J. Alloy. Compd. 647 (2015) 1061–1068, https://doi.org/10.1016/j.jallcom.2015.06.027.

[22] V. Russier, Blocking temperature of interacting magnetic nanoparticles with uniaxial and cubic anisotropies from Monte Carlo simulations, J. Magn. Magn. Mater. 409 (2016) 50–55, https://doi.org/10.1016/j.jmmm.2016.02.070.

[23] D.A. Balaev, S.V. Semenov, A.A. Dubrovskiy, S.S. Yakushkin, V.L. Kirillov, O. N. Martyanov, Superparamagnetic blocking of an ensemble of magnetite nanoparticles upon interparticle interactions, J. Magn. Magn. Mater. 440 (2017) 199–202.

[24] M. Vasilakaki, F. Gemenetzi, E. Devlin, D.K. Yi, S.N. Riduan, S.S. Lee, J.Y. Ying, G. C. Papaefthymiou, K.N. Trohidou, Size effects on the magnetic behavior of γ-Fe_2O_3 core/SiO_2 shell nanoparticle assemblies, 167570, J. Magn. Magn. Mater. 522 (2021), https://doi.org/10.1016/j.jmmm.2020.167570.

[25] K. Nadeem, M. Kamran, A. Javed, F. Zeb, S.S. Hussain, M. Mumtaz, H. Krenn, D. V. Szabo, U. Brossmann, X. Mu, Role of surface spins on magnetization of Cr_2O_3 coated γ-Fe_2O_3 nanoparticles, Solid State Sci. 83 (2018), https://doi.org/10.1016/j.solidstatesciences.2018.07.006.

[26] S.V. Komogortsev, V.A. Fel'k, O.A. Li, The magnetic dipole-dipole interaction effect on the magnetic hysteresis at zero temperature in nanoparticles randomly dispersed within a plane, J. Magn. Magn. Mater. 473 (2019) 410–415, https://doi.org/10.1016/j.jmmm.2018.10.091.

[27] S.V. Komogortsev, R.S. Iskhakov, V.A. Fel'k, Fractal dimension effect on the magnetization curves of exchange-coupled clusters of magnetic nanoparticles, J. Exp. Theor. Phys. 128 (2019) 754–760, https://doi.org/10.1134/S1063776119040095.

[28] L.L. Afremov, S.V. Anisimov, I.G. Iliushin, Modeling of the blocking temperature of a system of core/shell nanoparticles, Chin. J. Phys. 70 (2021) 324–335.

[29] M.S. Seehra, V.S. Babu, A. Manivannan, J.W. Lynn, Neutron scattering and magnetic studies of ferrihydrite nanoparticles, Phys. Rev. B. 61 (2000) 3513, https://doi.org/10.1103/PhysRevB.61.3513.

[30] L. Néel, Superantiferromagnetism in small particles, CR Acad. Sci. 253 (1961) 203–208.

[31] S. Mørup, D.E. Madsen, C. Frandsen, C.R.H. Bahl, M.F. Hansen, Experimental and theoretical studies of nanoparticles of antiferromagnetic materials, J. Phys. Condens. Matter 19 (2007), https://doi.org/10.1088/0953-8984/19/21/213202.

[32] A. Punnoose, T. Phanthavady, M.S. Seehra, N. Shah, G.P. Huffman, Magnetic properties of ferrihydrite nanoparticles doped with Ni, Mo, and Ir, Phys. Rev. B Condens. Matter Mater. Phys. 69 (2004), https://doi.org/10.1103/PhysRevB.69.054425.

[33] N.J.O. Silva, V.S. Amaral, L.D. Carlos, Relevance of magnetic moment distribution and scaling law methods to study the magnetic behavior of antiferromagnetic nanoparticles: Application to ferritin, Phys. Rev. B Condens. Matter Mater. Phys. 71 (2005), https://doi.org/10.1103/PhysRevB.71.184408.

[34] S.D. Tiwari, K.P. Rajeev, Effect of distributed particle magnetic moments on the magnetization of NiO nanoparticles, Solid State Commun. 152 (2012) 1080–1083, https://doi.org/10.1016/j.ssc.2012.03.003.

[35] A.A. Krasikov, D.A. Balaev, Analysis of Magnetization Processes in Antiferromagnetic Nanoparticles in Strong Pulse Fields (Brief Review), J. Exp. Theor. Phys. 136 (2023) 97–105, https://doi.org/10.1134/S1063776123010132.

[36] E.L. Duarte, R. Itri, E. Lima, M.S. Baptista, T.S. Berquó, G.F. Goya, Large magnetic anisotropy in ferrihydrite nanoparticles synthesized from reverse micelles, Nanotechnology 17 (2006) 5549, https://doi.org/10.1088/0957-4484/17/22/004.

[37] T.S. Berquó, J.J. Erbs, A. Lindquist, R.L. Penn, S.K. Banerjee, Effects of magnetic interactions in antiferromagnetic ferrihydrite particles, J. Phys. Condens. Matter 21 (2009) 176005, https://doi.org/10.1088/0953-8984/21/17/176005.

[38] Y.V. Knyazev, D.A. Balaev, S.V. Stolyar, A.A. Krasikov, O.A. Bayukov, M. N. Volochaev, R.N. Yaroslavtsev, V.P. Ladygina, D.A. Velikanov, R.S. Iskhakov, Interparticle magnetic interactions in synthetic ferrihydrite: Mössbauer spectroscopy and magnetometry study of the dynamic and static manifestations, J. Alloy. Compd. 889 (2022), https://doi.org/10.1016/j.jallcom.2021.161623.

[39] D.A. Balaev, S.V. Stolyar, Y.V. Knyazev, R.N. Yaroslavtsev, A.I. Pankrats, A. M. Vorotynov, A.A. Krasikov, D.A. Velikanov, O.A. Bayukov, V.P. Ladygina, R. S. Iskhakov, Role of the surface effects and interparticle magnetic interactions in the temperature evolution of magnetic resonance spectra of ferrihydrite nanoparticle ensembles, Results Phys. 35 (2022), https://doi.org/10.1016/j.rinp.2022.105340.

[40] Y.V. Knyazev, D.A. Balaev, R.N. Yaroslavtsev, A.A. Krasikov, D.A. Velikanov, Y. L. Mikhlin, M.N. Volochaev, O.A. Bayukov, S.V. Stolyar, R.S. Iskhakov, Tuning of the Interparticle interactions in ultrafine ferrihydrite nanoparticles, Adv, Nano Res 12 (2022), https://doi.org/10.12989/anr.2022.12.6.605.

[41] Y.V. Knyazev, D.A. Balaev, S.A. Skorobogatov, D.A. Velikanov, O.A. Bayukov, S. V. Stolyar, R.N. Yaroslavtsev, R.S. Iskhakov, Spin dynamics in ensembles of ultrafine ferrihydrite nanoparticles, Phys. Rev. B. 107 (2023), https://doi.org/10.1103/PhysRevB.107.115413.

[42] A.A. Krasikov, Y.V. Knyazev, D.A. Balaev, D.A. Velikanov, S.V. Stolyar, Y. L. Mikhlin, R.N. Yaroslavtsev, R.S. Iskhakov, Interparticle magnetic interactions and magnetic field dependence of superparamagnetic blocking temperature in ferrihydrite nanoparticle powder systems, 414901, Phys. B Condens. Matter 660 (2023), https://doi.org/10.1016/j.physb.2023.414901.

[43] Y.V. Knyazev, D.A. Balaev, S.V. Stolyar, O.A. Bayukov, R.N. Yaroslavtsev, V. P. Ladygina, D.A. Velikanov, R.S. Iskhakov, Magnetic anisotropy and core-shell structure origin of the biogenic ferrihydrite nanoparticles, 156753, J. Alloy. Compd. 851 (2021), https://doi.org/10.1016/j.jallcom.2020.156753.

[44] S.V. Stolyar, D.A. Balaev, V.P. Ladygina, A.A. Dubrovskiy, A.A. Krasikov, S. I. Popkov, O.A. Bayukov, Y.V. Knyazev, R.N. Yaroslavtsev, M.N. Volochaev, R. S. Iskhakov, K.G. Dobretsov, E.V. Morozov, O.V. Falaleev, E.V. Inzhevatkin, O. A. Kolenchukova, I.A. Chizhova, Bacterial Ferrihydrite Nanoparticles: Preparation, Magnetic Properties, and Application in Medicine, J. Supercond. Nov. Magn. 31 (2018), https://doi.org/10.1007/s10948-018-4700-1.

[45] D.A. Velikanov, SQUID MAGNETOMETER FOR INVESTIGATIONS OF THE MAGNETIC PROPERTIES OF MATERIALS IN THE TEMPERATURE RANGE 4, 2-370 K, Sib. Aerosp. J. 14 (2013) 176–181.

[46] A.D. Balaev, Y.V. Boyarshinov, M.M. Karpenko, B.P. Khrustalev, Automated magnetometer with superconducting solenoid, Instrum. Exp. Tech. (Engl. Transl.); (U. S.). 26 (1985).

[47] L. Gutiérrez, V. Barrón, M. Andrés-Vergés, C.J. Serna, S. Veintemillas-Verdaguer, M.P. Morales, F.J. Lázaro, Detailed magnetic monitoring of the enhanced magnetism of ferrihydrite along its progressive transformation into hematite, J. Geophys. Res. Solid Earth. 121 (2016) 4118–4129, https://doi.org/10.1002/2016JB013016.

[48] V.K. Anand, D.T. Adroja, A.D. Hillier, Ferromagnetic cluster spin-glass behavior in $PrRhSn_3$, Phys. Rev. B Condens. Matter Mater. Phys. 85 (2012), https://doi.org/10.1103/PhysRevB.85.014418.

[49] K. Binder, A.P. Young, Spin glasses: Experimental facts, theoretical concepts, and open questions, Rev. Mod. Phys. 58 (1986) 801, https://doi.org/10.1103/RevModPhys.58.801.

[50] D.A. Balaev, A.A. Krasikov, A.A. Dubrovskiy, S.I. Popkov, S.V. Stolyar, O. A. Bayukov, R.S. Iskhakov, V.P. Ladygina, R.N. Yaroslavtsev, Magnetic properties of heat treated bacterial ferrihydrite nanoparticles, J. Magn. Magn. Mater. 410 (2016), https://doi.org/10.1016/j.jmmm.2016.02.059.

[51] T.G.S. Pierre, P. Chan, K.R. Bauchspiess, J. Webb, S. Betteridge, S. Walton, D.P. E. Dickson, Synthesis, structure and magnetic properties of ferritin cores with varying composition and degrees of structural order: models for iron oxide deposits in iron-overload diseases, Coord. Chem. Rev. 151 (1996) 125–143, https://doi.org/10.1016/s0010-8545(96)90201-5.

[52] P. Gütlich, E. Bill, A.X. Trautwein, Mössbauer spectroscopy and transition metal chemistry: fundamentals and applications, Springer Science & Business Media,, 2010, https://doi.org/10.1007/978-3-540-88428-6.

[53] L.T. Kuhn, K. Lefmann, C.R.H. Bahl, S.N. Ancona, P.-A. Lindgård, C. Frandsen, D. E. Madsen, S. Mørup, Neutron study of magnetic excitations in 8−nm α−Fe_2O_3 nanoparticles, 184406, Phys. Rev. B. 74 (2006), https://doi.org/10.1103/PhysRevB.74.184406.

[54] C. Frandsen, S. Mørup, Spin Rotation in α−Fe_2O_3 Nanoparticles by Interparticle Interactions, 027202, Phys. Rev. Lett. 94 (2005), https://doi.org/10.1103/PhysRevLett.94.027202.

[55] H.H. Wickman, M.P. Klein, D.A. Shirley, Paramagnetic Hyperfine Structure and Relaxation Effects in Mössbauer Spectra: Fe 57 in Ferrichrome A, Phys. Rev. 152 (1966) 345, https://doi.org/10.1103/PhysRev.152.345.

[56] F. Van der Woude, A.J. Dekker, The relation between magnetic properties and the shape of Mössbauer spectra, Phys. Status Solid. (b 9 (1965) 775–786, https://doi.org/10.1002/pssb.19650090314.

[57] S. Mørup, B.R. Hansen, Uniform magnetic excitations in nanoparticles, 024418, Phys. Rev. B. 72 (2005), https://doi.org/10.1103/PhysRevB.72.024418.

[58] Z. Nemati, H. Khurshid, J. Alonso, M.H. Phan, P. Mukherjee, H. Srikanth, From core/shell to hollow Fe/γ-Fe_2O_3 nanoparticles: evolution of the magnetic behavior, Nanotechnology 26 (2015) 405705, https://doi.org/10.1088/0957-4484/26/40/405705.

[59] A.P. (A.P. Young, Spin glasses and random fields, World Scientific, (1998). ⟨https://cir.nii.ac.jp/crid/1130282273050084992.bib?lang=ja⟩ (accessed November 20, 2023).

[60] M. Orendáč, S. Lupínková, A. Doroshenko, E. Čižmár, A. Orendáčová, V. Švorčík, O. Lyutakov, D. Fajstavr, Z. Kolská, A. Zeleňáková, D. Peddis, Super spin-glass state in two-dimensional Fe_3O_4 nanoparticles deposited on a plasma-treated polymeric substrate, 104423, Phys. Rev. B. 108 (2023), https://doi.org/10.1103/PhysRevB.108.104423.

[61] J.A. Ramos-Guivar, E.C. Passamani, J. Litterst, Superspinglass state in functionalized zeolite 5A-maghemite nanoparticles, AIP Adv. 11 (2021), https://doi.org/10.1063/5.0038545.

[62] S. Nair, A.K. Nigam, Critical exponents and the correlation length in the charge exchange manganite spin glass Eu0.5Ba0.5MnO3, ArXiv Preprint Cond-Mat/0509360. (2005).

[63] V. Kumar, A. Sharma, Minakshi, R. Bhardwaj, A.K. Thukral, Temporal distribution, source apportionment, and pollution assessment of metals in the sediments of Beas river, India, Hum. Ecol. Risk Assess.: Int. J. 24 (2018) 2162–2181, https://doi.org/10.1080/10807039.2018.1440529.

[64] N.J.O. Silva, A. Millan, F. Palacio, E. Kampert, U. Zeitler, H. Rakoto, V.S. Amaral, Temperature dependence of antiferromagnetic susceptibility in ferritin, 104405, Phys. Rev. B. 79 (2009), https://doi.org/10.1103/PhysRevB.79.104405.

[65] D.A. Balaev, S.I. Popkov, A.A. Krasikov, A.D. Balaev, A.A. Dubrovskiy, S.V. Stolyar, R.N. Yaroslavtsev, V.P. Ladygina, R.S. Iskhakov, Temperature behavior of the antiferromagnetic susceptibility of nanoferrihydrite from the measurements of the magnetization curves in fields of up to 250 kOe, Phys. Solid State 59 (2017) 1940–1946.

[66] S.I. Popkov, A.A. Krasikov, D.A. Velikanov, V.L. Kirillov, O.N. Martyanov, D. A. Balaev, Formation of the magnetic subsystems in antiferromagnetic NiO nanoparticles using the data of magnetic measurements in fields up to 250 kOe, J. Magn. Magn. Mater. 483 (2019) 21–26, https://doi.org/10.1016/j.jmmm.2019.03.004.

[67] R.H. Kodama, A.E. Berkowitz, Atomic-scale magnetic modeling of oxide nanoparticles, Phys. Rev. B Condens. Matter Mater. Phys. 59 (1999), https://doi.org/10.1103/PhysRevB.59.6321.

[68] D.A. Balaev, A.A. Krasikov, S.I. Popkov, A.A. Dubrovskiy, S.V. Semenov, D. A. Velikanov, V.L. Kirillov, O.N. Martyanov, Features of the quasi-static and dynamic magnetization switching in NiO nanoparticles: Manifestation of the interaction between magnetic subsystems in antiferromagnetic nanoparticles, J. Magn. Magn. Mater. 515 (2020) 167307.

[69] C.T. Meneses, J.G.S. Duque, E. De Biasi, W.C. Nunes, S.K. Sharma, M. Knobel, Competing interparticle interactions and surface anisotropy in NiO nanoparticles, 013909, J. Appl. Phys. 108 (2010), https://doi.org/10.1063/1.3459890.

[70] E. De Biasi, C.A. Ramos, R.D. Zysler, H. Romero, Ferromagnetic resonance in amorphous nanoparticles, Phys. B Condens. Matter 354 (2004) 286–289, https://doi.org/10.1016/j.physb.2004.09.103.

[71] F.G. da Silva, J. Depeyrot, Y.L. Raikher, V.I. Stepanov, I.S. Poperechny, R. Aquino, G. Ballon, J. Geshev, E. Dubois, R. Perzynski, Exchange-bias and magnetic anisotropy fields in core–shell ferrite nanoparticles, Sci. Rep. 11 (2021) 5474, https://doi.org/10.1038/s41598-021-84843-0.

[72] B. René, B. Jean-Claude, K. Janis, Lineshapes in magnetic resonance spectra, (2000). https://doi.org/10.1088/0953–8984/12/44/315.

[73] J. Landers, F. Stromberg, M. Darbandi, C. Schöppner, W. Keune, H. Wende, Correlation of superparamagnetic relaxation with magnetic dipole interaction in capped iron-oxide nanoparticles, J. Phys. Condens. Matter 27 (2014) 026002, https://doi.org/10.1088/0953-8984/27/2/026002.

[74] F. Gazeau, J.C. Bacri, F. Gendron, R. Perzynski, Y.L. Raikher, V.I. Stepanov, E. Dubois, Magnetic resonance of ferrite nanoparticles:: evidence of surface effects, J. Magn. Magn. Mater. 186 (1998) 175–187, https://doi.org/10.1016/S0304-8853(98)00080-8.

[75] R. Berger, J.-C. Bissey, J. Kliava, H. Daubric, C. Estournès, Temperature dependence of superparamagnetic resonance of iron oxide nanoparticles, J. Magn. Magn. Mater. 234 (2001) 535–544.

[76] M. Rubinstein, R.H. Kodama, S.A. Makhlouf, Electron spin resonance study of NiO antiferromagnetic nanoparticles, J. Magn. Magn. Mater. 234 (2001) 289–293, https://doi.org/10.1016/S0304-8853(01)00313-4.

[77] N.E. Domracheva, A.V. Pyataev, R.A. Manapov, M.S. Gruzdev, Magnetic Resonance and Mössbauer Studies of Superparamagnetic γ-Fe_2O_3 Nanoparticles Encapsulated into Liquid-Crystalline Poly (propylene imine) Dendrimers, ChemPhysChem 12 (2011) 3009–3019, https://doi.org/10.1002/cphc.201100363.

[78] C. Antoniak, J. Lindner, M. Farle, Magnetic anisotropy and its temperature dependence in iron-rich Fe_xPt_{1-x} nanoparticles, Europhys. Lett. 70 (2005) 250.

[79] S.S. Yakushkin, A.A. Dubrovskiy, D.A. Balaev, K.A. Shaykhutdinov, G. A. Bukhtiyarova, O.N. Martyanov, Magnetic properties of few nanometers ε-Fe_2O_3, Nanopart. Support. silica, J. Appl. Phys. 111 (2012) 044312.

[80] A.I. Pankrats, A.M. Vorotynov, V.I. Tugarinov, S.M. Zharkov, G.M. Zeer, K. Ramasamy, A. Gupta, Magnetic resonance studies of mixed chalcospinel $CuCr_2S_xSe_{4-x}$ (x = 0; 2) and $Co_xCu_{1-x}Cr_2S_4$ (x = 0.1; 0.2) nanocrystals with strong interparticle interactions, J. Magn. Magn. Mater. 452 (2018) 297–305, https://doi.org/10.1016/j.jmmm.2017.12.092.

[81] A.I. Pankrats, A.M. Vorotynov, V.I. Tugarinov, S.M. Zharkov, D.A. Velikanov, G. M. Abramova, G.M. Zeer, K. Ramasamy, A. Gupta, Structural and magnetic resonance investigations of $CuCr_2S_4$ nanoclusters and nanocrystals, 054302, J. Appl. Phys. 116 (2014), https://doi.org/10.1063/1.4891993.

[82] I.S. Edelman, S.M. Zharkov, A.I. Pankrats, A.M. Vorotynov, V.I. Tugarinov, R. D. Ivantsov, D.A. Petrov, D.A. Velikanov, C.-R. Lin, C.-C. Chen, Electron spin resonance in $Cu_{1-x}Fe_xCr_2Se_4$ nanoparticles synthesized with the thermal decomposition method, J. Magn. Magn. Mater. 436 (2017) 21–30, https://doi.org/10.1016/j.jmmm.2017.04.006.

[83] S.V. Stolyar, R.N. Yaroslavtsev, R.S. Iskhakov, O.A. Bayukov, D.A. Balaev, A. A. Dubrovskii, A.A. Krasikov, V.P. Ladygina, A.M. Vorotynov, M.N. Volochaev, Magnetic and resonance properties of ferrihydrite nanoparticles doped with cobalt, Phys. Solid State 59 (2017) 555–563, https://doi.org/10.1134/S1063783417030301.

[84] I.V. Yakovlev, S.S. Yakushkin, M.A. Kazakova, S.N. Trukhan, Z.N. Volkova, A. P. Gerashchenko, A.S. Andreev, A.V. Ishchenko, O.N. Martyanov, O.B. Lapina, Superparamagnetic behaviour of metallic Co nanoparticles according to variable temperature magnetic resonance, Phys. Chem. Chem. Phys. 23 (2021) 2723–2730, https://doi.org/10.1039/d0cp05963c.

[85] S.V. Stolyar, D.A. Balaev, V.P. Ladygina, A.I. Pankrats, R.N. Yaroslavtsev, D. A. Velikanov, R.S. Iskhakov, Ferromagnetic resonance study of biogenic ferrihydrite nanoparticles: spin-glass state of surface spins, JETP Lett. 111 (2020) 183–187, https://doi.org/10.1134/S0021364020030145.

[86] K.Y. Sova, A.S. Vakula, S.I. Tarapov, A.G. Belous, S.O. Solopan, Analysis of low-temperature FMR spectra of Fe_3O_4 and $ZnFe_2O_4$ nanoparticles synthesized using organic molecules, Low. Temp. Phys. 47 (2021) 220–227, https://doi.org/10.1063/10.0003522.

[87] A. Punnoose, M.S. Seehra, J. Van Tol, L.C. Brunel, High-frequency electron magnetic resonance and magnetic studies of ferrihydrite nanoparticles and evidence of a phase transition, J. Magn. Magn. Mater. 288 (2005) 168–172, https://doi.org/10.1016/j.jmmm.2004.09.003.

[88] M. Wencka, A. Jelen, M. Jagodič, V. Khare, C. Ruby, J. Dolinšek, Magnetic and EPR study of ferric green rust-and ferrihydrite-coated sand prepared by different synthesis routes, J. Phys. D. Appl. Phys. 42 (2009) 245301, https://doi.org/10.1088/0022-3727/42/24/245301.

[89] S.V. Yurtaeva, V.N. Efimov, N.I. Silkin, A.A. Rodionov, M.V. Burmistrov, A. V. Panov, A.A. Moroshek, Magnetic resonance of ferritin crystalline particles in tumor tissue, Appl. Magn. Reson. 42 (2012) 299–311, https://doi.org/10.1007/s00723-012-0312-2.

[90] E. Mosiniewicz-Szablewska, A. Ślawska-Waniewska, K. Świątek, N. Nedelko, J. Galązka-Friedman, A. Friedman, Electron paramagnetic resonance studies of human liver tissues, Appl. Magn. Reson. 24 (2003) 429–435, https://doi.org/10.1007/BF03166946.

[91] S.K. Misra, S.I. Andronenko, S. Asthana, D. Bahadur, A variable temperature EPR study of the manganites $(La_{1/3}Sm_{2/3})_{2/3}Sr_xBa_{0.33-x}MnO_3$ (x = 0.0, 0.1, 0.2, 0.33): Small polaron hopping conductivity and Griffiths phase, J. Magn. Magn. Mater. 322 (2010), https://doi.org/10.1016/j.jmmm.2010.05.003.

[92] G.F. Goya, T.S. Berquo, F.C. Fonseca, M.P. Morales, Static and dynamic magnetic properties of spherical magnetite nanoparticles, J. Appl. Phys. 94 (2003) 3520–3528, https://doi.org/10.1063/1.1599959.

[93] anon.